Determining the Feasibility of Cyclic Voltammetry for Pyroprocessing Safeguards

A Thesis Presented for the

Master of Science

Degree

The University of Tennessee, Knoxville

Jonathan Trent Mitchell

August 2020

Copyright © by Jonathan Trent Mitchell, 2020
All Rights Reserved.

This thesis is dedicated to my family and friends. Without their encouragement and assistance along the way, this would not have been possible.

Acknowledgments

This work would not have been possible without the help I received from those around me along the way. I would first like to thank my family, who supported me while working towards my degree. I would not have been able to do this without them.

I would also like to thank my advisors. They have been instrumental in providing me both the resources and education needed to complete this work. Thanks goes to Dr. Steve Skutnik and Dr. Jamie Coble for being patient and pleasant to work with during the course of my thesis work.

My coworkers have also been very helpful during my time working on this degree. I would like to thank Nathan Gilliam, Michael Cooper, Amanda Bachmann, and Jonathan Wing. They were all great to work alongside, and willing to offer assistance when needed.

I would also like to thank the team at Sandia National Lab, for providing the SSPM model which generated some of the data used with the model for this report.

Abstract

Cyclic Voltammetry (CV) has been under recent consideration for assessing the bulk uranium content in the electrorefiner used in pyroprocessing. Many prior studies have focused on either measuring the cell's electrochemical characteristics, or were limited to a small number of different electrorefiner contents. This study however focuses on assessing CV for predicting the cell's uranium content with a wide array of cell contents. To do this, a simplified CV model was used on electrorefiner content data from a pyroprocessing flowsheet model and on data covering a uranium mass fraction range of 0.25% to 10.0%. Linear trends were evaluated in the CV output from the model (irreversible peak current difference) under these two ranges. A 7% maximum relative error was observed between the model's CV output and the predicted output from the trend for the data covering uranium weight percents from 0.25 wt% to 10.0 wt%, and 1.97% for the data from the flowsheet model. These trends were then used to reverse-correlate back to uranium weight percent in the electrorefiner. A maximum error of 1.90% between the reverse-correlated and actual uranium weight percent was reported for the flowsheet data. Further analysis was performed to measure the uncertainty in the evaluated linear trends in the CV output, including measuring the impact of data size and data noise. Increasing the data size decreased uncertainty in the linear regressions' slope and intercept values found via the CV model, and increasing the CV output noise significantly increased these regression uncertainties. Data noise had a roughly linear contribution to regression uncertainty (e.g. 15% data noise resulted in 3 times the regression uncertainty of 5% noise, assuming the same data size), while data size had a somewhat lesser effect. When these trends were used to reverse-correlate from the CV output back to uranium mass percent, data noise proved to have the largest impact on accuracy, with maximum prediction error increasing to 40-50% at the extreme error values. These results illustrate that cyclic

voltammetry can produce viable results for monitoring the electrorefiner uranium content, so long as any potential biases within the system are mitigated.

Table of Contents

1 Introduction **1**

2 Background **3**

2.1 Pyroprocessing 3

2.2 Cyclic Voltammetry 6

2.3 Voltammetric Studies 9

3 Methods **13**

4 Results **22**

5 Summary and Future Work **35**

Bibliography **39**

Appendices **43**

A Miscellaneous Figures 44

B Miscellaneous Tables 52

C MATLAB Codes 54

C.1 Initialize_CV_Data.m 54

C.2 Trim_Data.m 59

C.3 CV_Data_Select.m 60

C.4 SweepTest.m 63

C.5 Data_Sweep.m 65

C.6 CV_Plotting.m 66

C.7 Extrapolation_Plots.m 68
C.8 Stepwise_Fit.m 70
C.9 Gen_Fit_Uncertainty.m 71

Vita **79**

List of Tables

2.1 Expected Measurement Uncertainty (Values taken from [4]) 6

3.1 Table of input values used for generating CV traces within SSPM. This data is used both for interpolation and extrapolation purposes between the given concentrations of uranium. 18

3.2 List of Extrapolation Methods used for each variable in the CV input data. . 21

4.1 Linear Trends used for Correlating CV Peak Difference and Uranium Weight Percent. 25

4.2 Slopes, Intercepts, and Associated Uncertainties for Each Region Using 100 Points With 5% Data Noise. 28

4.3 Slopes, Intercepts, and Associated Uncertainties for Each Region Using 500 Points With 5% Data Noise. 28

4.4 Slopes, Intercepts, and Associated Uncertainties for Each Region Using 200 Points With 5% Data Error. 30

4.5 Slopes, Intercepts, and Associated Uncertainties for Each Region Using 200 Points With 15% Data Error. 30

4.6 Mean Error in Prediction of Uranium Weight Percent for Different Data Noise Values and Data Sizes Over the Range of 0.25 wt% to 10.0 wt%. 33

4.7 Average Maximum Error in Prediction of Uranium Weight Percent for Different Data Noise Values and Data Sizes Over the Range of 0.25 wt% to 10.0 wt%. 33

B.1 Slopes, Intercepts, and Associated Uncertainties for Each Region Using 100 Points With 10% Data Noise. 52
B.2 Slopes, Intercepts, and Associated Uncertainties for Each Region Using 100 Points With 15% Data Noise. 52
B.3 Slopes, Intercepts, and Associated Uncertainties for Each Region Using 200 Points With 10% Data Noise. 52
B.4 Slopes, Intercepts, and Associated Uncertainties for Each Region Using 500 Points With 10% Data Noise. 53
B.5 Slopes, Intercepts, and Associated Uncertainties for Each Region Using 500 Points With 15% Data Noise. 53

List of Figures

2.1 Layout of the pyroprocessing flowsheet developed by Argonne National Laboratory [1]. 5

2.2 Potential vs. time during a CV measurement, using a scan rate of 100 mV/s. [3]. 8

3.1 Cyclic Voltammogram for a 2.5 wt% UCl_3 solution in LiCl-KCl eutectic salt at 773 K. Data is generated using 200 $\frac{mV}{s}$ scan rate [13]. 14

3.2 Cyclic Voltammogram for a 2.5 wt% UCl_3 solution. This illustrates how much data was cut off in order to improve efficiency during simulation run-time. . 16

3.3 Example plot of input data suitable for a linear extrapolation into the low U wt% region. The linear trend used for such extrapolation is included for comparison with the data. This data is for the surface area at the electrode. 20

3.4 Example plot of input data suitable for a constant extrapolation into the low U wt% region. This data is for the formal electrode potential within the cathodic reversible region. 20

4.1 Plot of the peak current difference vs. uranium weight percent from 0.25 wt% to 10 wt%. 23

4.2 Plot of the peak current difference vs. uranium weight percent from 0.25 wt% to 10 wt%. A plot of the trendlines used in each region is used for comparison. 24

4.3 Plot of the CV peak difference vs. uranium weight percent for the range of data calculated with a 15000 hour SSPM. The fuel input had a cooling time of 5 years, was 2.17% enriched, and had a burnup of 20 GWd/MTU. Trendlines are included for comparison. 26

4.4 Plot of the predicted and actual uranium weight percent over time. From this, we see that the predictions mach closely with the actual content within the electrorefiner. 27
4.5 Plot of z-scores for slope and intercept values for each region. The spreads look very similar after being normalized here, but considering that each region has different standard deviations for their individual slopes and intercepts, we know that the regions with high uncertainties in their measured trends exhibit much more spread, despite having the same shape as the rest. 32
4.6 Plot of z-scores for slope and intercept values for each region as a heat map. 32

A.1 Example plot of data suitable for a linear extrapolation into the low U wt% region. The linear trend used for such extrapolation is included for comparison with the data. This data is for the diffusion coefficient of the oxidized species on the irreversible side. 44
A.2 Example plot of data suitable for a linear extrapolation into the low U wt% region. The linear trend used for such extrapolation is included for comparison with the data. This data is for the diffusion coefficient of the oxidized species on the reversible side. 45
A.3 Example plot of data suitable for a linear extrapolation into the low U wt% region. The linear trend used for such extrapolation is included for comparison with the data. This data is for the diffusion coefficient of the reduced species on the irreversible side. 45
A.4 Example plot of data suitable for a linear extrapolation into the low U wt% region. The linear trend used for such extrapolation is included for comparison with the data. This data is for the diffusion coefficient of the reduced species on the reversible side. 46
A.5 Example plot of data suitable for a linear extrapolation into the low U wt% region. The linear trend used for such extrapolation is included for comparison with the data. This data is for the formal electrode potential on the anodic reversible side. 46

A.6 Example plot of data suitable for a linear extrapolation into the low U wt% region. The linear trend used for such extrapolation is included for comparison with the data. This data is for the formal electrode potential on the anodic irreversible side. 47
A.7 Example plot of data suitable for a linear extrapolation into the low U wt% region. The linear trend used for such extrapolation is included for comparison with the data. This data is for the formal electrode potential on the cathodic irreversible side. 47
A.8 Example plot of data suitable for a linear extrapolation into the low U wt% region. The linear trend used for such extrapolation is included for comparison with the data. This data is for the scan rate. 48
A.9 Example plot of data suitable for a linear extrapolation into the low U wt% region. The linear trend used for such extrapolation is included for comparison with the data. This data is for the initial time. 48
A.10 Example plot of data suitable for a linear extrapolation into the low U wt% region. The linear trend used for such extrapolation is included for comparison with the data. This data is for the time interval between points on the CV scan. 49
A.11 Example plot of data suitable for a linear extrapolation into the low U wt% region. The linear trend used for such extrapolation is included for comparison with the data. This data is for the time spent on the anodic irreversible side. 49
A.12 Example plot of data suitable for a linear extrapolation into the low U wt% region. The linear trend used for such extrapolation is included for comparison with the data. This data is for the time spent on the cathodic irreversible side. 50
A.13 Example plot of data suitable for a linear extrapolation into the low U wt% region. The linear trend used for such extrapolation is included for comparison with the data. This data is for the time spent on the anodic reversible side. . 50
A.14 Example plot of data suitable for a linear extrapolation into the low U wt% region. The linear trend used for such extrapolation is included for comparison with the data. This data is for the time spent on the cathodic reversible side. 51

Chapter 1

Introduction

Pyroprocessing has been a prospective reprocessing technique under consideration as an alternative to aqueous reprocessing. While both methods are used to increase utilization of used nuclear fuel by separating uranium and plutonium from reactor fuel, each relies upon a different mechanism for separation, and each have different physical environments in which they operate. Pyroprocessing, for example, is a batch process, versus a continuous aqueous reprocessing methodology, which can lead to a buildup of material within the plant. In addition, pyroprocessing involves comingling highly radioactive fission products, corrosive molten salts, and high temperatures all within the electrorefiner alone. As such, since the physical characteristics of the separation environment are unique between the aqueous and pyroprocessing separation schemes, a new regime must be used for monitoring the concentration of important nuclides within a pyroprocessing plant. This monitoring is especially important within the electrorefiner, as this is where the fissile nuclides from used nuclear fuel are separated from the remaining fuel material. Knowing this, cyclic voltammetry (CV) has been under consideration, as this method can be used to measure the uranium concentration within the electrorefiner. This could prove to be an essential component within a pyroprocessing plant for both safeguards and material accountancy if its performance proves it viable. This report discusses the feasibility of this measurement method for this purpose.

While other studies have used CV to study the electrochemical behavior within an electrorefiner, this study expands on prior research by using a model to simulate a CV

trace, which is then used to reverse-correlate the uranium concentration given data regarding the elemental contents of the electrorefiner. This report also looks into evaluating the uncertainty of any trends discovered between uranium concentration and the CV results, and the impact of noise in the data and data size on these trends. These would be important considerations to make when attempting to reverse-correlate the uranium concentration within the electrorefiner from the results of the CV measurement. A more thorough overview of the relevant literature is given in section 2.3.

This work is part of a larger Nuclear Energy University Program (NEUP) project which includes discussion of other measurements for pyroprocessing, and several of the results for the cyclic voltammetry portion of that report are included here [2].

Chapter 2

Background

2.1 Pyroprocessing

Pyroprocessing is a novel reprocessing technique under active research as an alternative to aqueous (PUREX) reprocessing. Unlike aqueous methods, pyroprocessing relies on separating uranium, plutonium, and other elements from used fuel via an electrochemical process, which necessitates unique operating conditions to those of PUREX. To provide context for ideas discussed in this report, a brief introduction to pyroprocessing is included here.

Pyroprocessing can be split into five major processing areas: fuel preparation, oxide-to-metal conversion, actinide/fission product separations, material recycle, and waste treatment [1]. Once fuel enters into the facility, the fuel assemblies are disassembled mechanically, and the cladding material is removed to reduce the volume and alleviate some front-end chemistry challenges [1]. Following this, an optional voloxidizer stage is sometimes employed to further process the fuel. During this stage, the fuel is reacted with oxygen or air to form tri-uranium octoxide (U_3O_8) powder [19]. This stage allows for the removal of noble gases and some volatile fission products (such as cesium and ruthenium) and also increases the surface area of the fuel, allowing for improved reaction kinetics in the electroreduction stage [18]. Once complete, the fuel then undergoes electrolyltic reduction, which reduces the oxide fuel into a metallic form using lithium as a reducing agent. This is done by using either lithium metal dissolved in LiCl (as has been done in the past), or with a $LiCl - Li_2O$ electrolyte (under

more recent consideration) [6]. Either way, this leaves the fuel in a metallic form compatible with the electrorefiner [18].

From here, the reduced used fuel enters the electrorefiner, where uranium product and optionally transuranic (TRU)/uranium product are codeposited from the fission products. The spent fuel (which acts as the anode) is inserted into a eutectic salt (usually LiCl and KCl), and a potential is passed between the anode and cathode. This drives the electrotransport of these two aforementioned product streams onto their respective cathodes [17] (one solid cathode for the uranium product, another liquid cathode for the TRU/uranium product). The remaining fission products and noble metals lie either as chlorides in the salt or remain on the anode basket respectively [1]. The chemistry behind this separation technique lies in the elements' unique Gibbs free energy of chloride formation. Alkali and alkaline earth fission products are very stable as chlorides in the salt and are not drawn out of the electrorefiner despite the current between the anode and cathode. The noble metals are not stable in chloride form, and so remain as metals on the anode. Uranium and the transuranics however, lie between these two extremes. As such, they can be drawn out onto the cathode via the passage of current after being drawn into the salt as chlorides [9].

Once the U and TRU/U products are drawn out of the electrorefiner, they undergo further processing to remove the remaining salt prior to ingot casting. For the uranium product stream, salt is removed via distillation in the cathode processor [18], and for the TRU/U stream, salt is separated by melting the alloy and separating the metal from the salt via the discrepancy in their densities. From there, the two products are cast into ingots for storage and later use [1]. A detailed illustration of this pyroprocessing flowsheet is given in Figure 2.1.

Some pyroprocessing flowsheets include extra steps in addition to the basics previously discussed. For example, KAERI's (Korea Atomic Energy Research Institute) flowsheet includes not only the optional voloxidizer, but also an electrolytic cathode processor integrated into their flowsheet following reduction. This stage is designed to remove some of the salt used in the reduction step (since it adversely affects the electrolytic reduction step) [10].

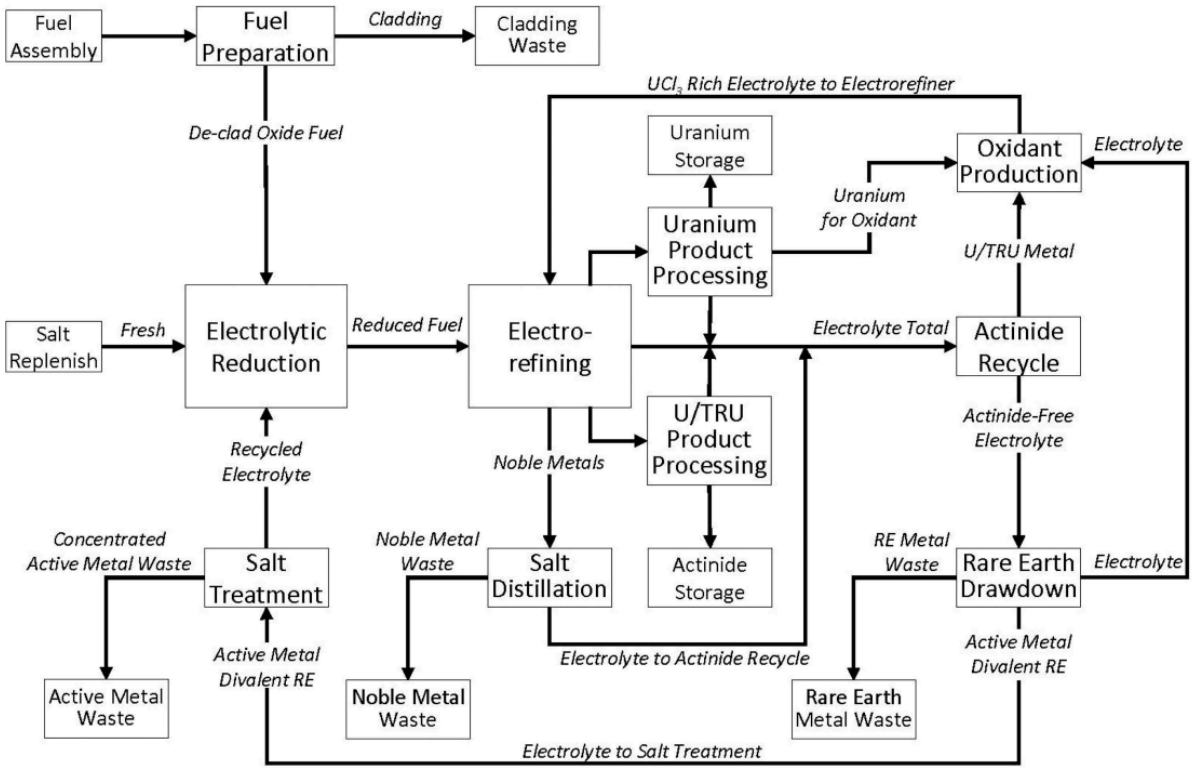


Figure 2.1: Layout of the pyroprocessing flowsheet developed by Argonne National Laboratory [1].

This reprocessing technique presents unique challenges not only for safeguards, but also for material accountancy. The International Atomic Energy Agency (IAEA) stipulates that one significant quantity of fissile material (roughly the amount of fissile material to create a thermonuclear weapon) must be detected within 1 month of diversion [4]. In addition, the IAEA has strict requirements for uncertainties with measurements for reprocessing technology (detailed in Table 2.1) [4], and considering that pyroprocessing facilities are not designed to have frequent plant flushouts (where the plant is shut down and all nuclear material assayed) [8], accurate, low-latency (i.e. low result turnaround time) measurement techniques that can be used while the facility is online will be needed to satisfy all of the IAEA requirements for these facilities. It is unlikely that these requirements will all be satisfied solely via one measurement method. Instead, it is more feasible to develop a safeguards strategy that relies on the results of many measurements to reduce overall assay uncertainty,

Table 2.1: Expected Measurement Uncertainty (Values taken from [4])

Measurement	Expected Relative Uncertainty
Uranium Enrichment	0.002
Uranium Fabrication	0.003
Plutonium Fabrication	0.005
Uranium Reprocessing	0.008
Plutonium Reprocessing	0.01
Separate Scrap Storage	0.04
Separate Waste Storage	0.25

and is why cyclic voltammetry is being considered as an additional measurement technique to include in such a safeguards regime.

Beyond simply reducing material uncertainty, having multiple assay techniques will reduce the likelihood that a potential proliferator could fool each measurement into reading a supposedly normal value. If only one measurement were used, the assayed material could be constructed/designed in a way to trick the detection system. Multiple measurement techniques would reduce the chance of such spoofing. An example of this concept would be constructing a fissile sample with highly-enriched uranium (HEU) towards the center of the sample and low-enriched uranium (LEU) on the edge. Such a construction could fool a gamma measurement of enrichment when used alone (due to self-shielding), but if neutron measurements were also used for enrichment detection, the system would be less susceptible to this form of spoofing.

2.2 Cyclic Voltammetry

Cyclic voltammetry (CV) is a promising method for monitoring pyroprocessing which can be used to assess the elemental contents within an electrochemical cell. Namely, for this process, CV is capable of characterizing the elemental concentration of uranium within the a molten salt eutectic (such as that salt within the electrorefiner). While alone, this measurement is not capable of performing a full assay of the contents within the electrochemical cell, it

can be coupled along with other measurements to obtain either a more accurate, or more complete analysis of the cell's contents.

An elemental assay of the uranium content within the electrofiner (such as that provided by CV) is crucial to not only ensuring the plant is operating as expected, but for also detecting any foul play. As the electrorefiner is where actinide separation occurs, uranium is left in a much more pure form upon leaving the electrochemical cell, leaving it a more viable target for theft. As such, being able to compare the uranium content within the electrorefiner versus the uranium content entering the cathode processor (the next step in uranium purification) is essential for determining if there is any material unaccounted for (MUF). Measuring the difference between uranium content at these two points would allow for detection of any uranium buildup within the cell (a material accountancy issue), and would also enable the detection of uranium theft from the electrorefiner (a safeguards issue).

The CV technique itself involves linearly ramping the potential within the cell from one potential to another, and then linearly ramping back to the original potential. Ramping the potential in such a way triggers oxidative and anodic reactions within the cell, both of which result in a measurable current that can be traced back to the uranium concentration within the cell. The rate at which the voltage is changed during the process is known as the scan rate, ν, and is constant for a given measurement. A graphical representation of this voltage ramp is shown in Figure 2.2 [3].

In order to calculate the CV trace of current versus potential, the reverse-engineering calculational method described by Phongikaroon and Pouri was adopted and modified for use with this analysis [13]. The method itself involves the following two general forms of the Randles-Sevcik equation, detailed in equations 2.1 and 2.2 [12]. For a reversible reaction, ψ is given by equation 2.3, and for an irreversible reaction, it is given by equation 2.4. More specifically, the $\pi\chi(\phi t)$ term is referred to as the "Randles-Sevcik" equation for a reversible reaction, and as the "Delahay" equation for an irreversible one. In these equations, i is current (A) n is the number of electrons transferred per mole $(\frac{eq}{mol})$, F is Faraday's constant, A is the surface area of the working electrode (cm^2), C_0^* is the bulk concentration of oxidized species $(\frac{mol}{cm^3})$, D_0 is the diffusion coefficient of oxidized species$(\frac{cm^2}{s})$, t is time (s), C_R^* is the bulk concentration of reduced species $(\frac{mol}{cm^3})$, D_R is the diffusion coefficient of reduced species

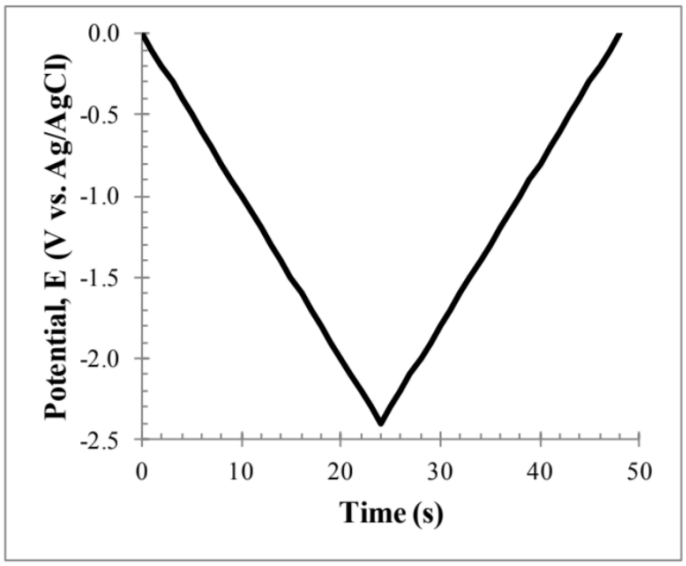


Figure 2.2: Potential vs. time during a CV measurement, using a scan rate of 100 mV/s. [3].

($\frac{cm^2}{s}$), α is the transfer coefficient (usually 0.5), R is the universal gas constant, T is the absolute temperature (K), ν is the scan rate ($\frac{V}{s}$), E_i is the initial potential (V), and E is the potential (V). Also of concern is the formal electrode potential, E_0 (V) [14].

Both of these equations, when used in conjunction, can be used to find current at different times, and therefore, the CV trace. Input data for the model, including the uranium concentration, diffusion coefficients and other constants detailed in the aforementioned equations, are derived from a table detailed in Pouri's report (Table 3.2 in the report), which is used for interpolating between the discrete uranium concentrations (1 wt%, 2.5 wt%, 5 wt%, 7.5 wt%, and 10 wt%) within the table. Not all of the data in the table was used for our purposes, the reasons for which are detailed later in the report. Extra detail on how these equations are used to generate the CV traces is given in [12, 13, 14], and Nicholson and Shain have delved far into the theory [11].

$$i_{reversible} = nFAC_0^* \sqrt{\pi D_0 \psi} \chi(\psi t) \tag{2.1}$$

$$i_{irreversible} = nFAC_R^* \sqrt{\pi D_R \alpha \psi} \chi(\alpha \psi t) \tag{2.2}$$

$$\psi_{reversible} = \frac{nF}{RT} \nu t = \frac{nF}{RT} E_i - E \tag{2.3}$$

$$\psi_{irreversible} = \frac{n\alpha F}{RT} \nu t = \frac{n\alpha F}{RT} E_i - E \tag{2.4}$$

2.3 Voltammetric Studies

Several studies have been conducted before on the uranium electrochemistry within a LiCl-KCl eutectic. Hoover conducted such studies alongside research for zirconium chemistry in 2014 using the Mk-IV electrorefiner located at INL [3]. The primary findings of their research was in measuring the diffusion and apparent standard reduction potentials for uranium and zirconium for their system. One of the other results of their study was a linear correlation between uranium concentration and CV peak current density, which produced a reasonable fit with an R^2 of almost 0.8 for an anodic current and 0.96 for the cathodic current using 5 different uranium concentrations within their electrochemical cell. These studies also looked into specific measurement concerns, such as how scan rate and diffusion coefficients influence the results obtained from a CV scan. Hoover also reported that having a significant quantity of zirconium in a system with uranium would interfere with a CV measurement due to the extra redox reactions which occur with zirconium. When zirconium is present in such concentrations, a deconvolution method may be required to properly distinguish the redox peaks from both elements [3].

Johnson also performed research in voltammetric techniques, testing whether square-wave or normal pulse voltammetry proved better for their $LiCl - KCl - UCl_3 - PuCl_3$ system [5].

While these are not studies for cyclic voltammetry, the procedure for implementing them is similar, and so their research is relevant to the success of CV in such systems.

To get a better understanding of the underlying physics within the electrorefiner, Kim et al. analyzed data taken from cyclic voltammetry to measure key underlying physical parameters, like the formal electrode potential and diffusion coefficient of U^{3+} [7]. Their study was able to quantify the formal electrode potential and diffusion coefficient for uranium for their LiCl-KCl system at 773 K. While not a direct uranium measurement, these quantities are essential not only to perform optimal simulations of CV, but also to correlate any results taken from CV with uranium content.

Phongikaroon's simplified CV model has proven successful in the past for generating CV traces, resulting in strong agreement with the results from Hoover's studies [12]. The model has also shown some success when implemented for analyzing zirconium CV traces [13]. These points indicate that the model's algorithm is sound and its use is justified for this work for assessing CV's feasibility for pyroprocessing safeguards and material accountancy within the electrorefiner.

In a similar vein, Pouri, Manic, and Phongikaroon also developed an artificial neural network (ANN) which could predict the output of a CV measurement for electrorefiner systems with zirconium. They used over 230,000 experimental datapoints within the 0.5-5 wt% zirconium range from an LiCl-KCl system at 773 K. One of their ANN structures was able to replicate the CV traces with an root mean square error (RMSE) of 5% or less when compared to the experimental traces. This study illustrates the relevance of ANNs and the underlying cyclic voltammetry method to pyroprocessing safeguards research [15].

Lastly, Rappleye, Newton, Zhang, and Simpson [16] have also done analysis on LiCl-KCl electrorefiner systems containing magnesium and uranium. Several voltammetric techniques were tested, including cyclic voltammetry, choronoamperometry (CA), open-circuit potential (OCP) and normal pulse voltammetry (NPV). Their studies analyzed the viability of using $MgCl_2$ as a surrogate for $PuCl_3$ in the system, so that a greater range of concentrations could be attained [16]. Their work showed the viability of using the $MgCl_2$ surrogate, and CV proved a capable measurement, exhibiting strong linear correlations between uranium

and magnesium concentration and their respective peak current values (R^2 of 0.954 for magnesium and 0.919 for uranium).

While all of these studies are relevant for assessing the use of CV for pyroprocessing safeguards, there are gaps in the prior research which warrant additional investigation. Many of these prior studies on cyclic voltammetry were limited in some aspect. Hoover's study only collected CV data on a limited number of different uranium concentrations [3]. The CV model developed by Phongikaroon (which was adopted here) was tested by comparing its output to the traces gathered experimentally, but its use in correlating its output back to the electrorefiner uranium content was not heavily investigated [13]. The ANN developed to predict CV traces was only tested on zirconium data. In addition, many of the studies conducted here were primarily focused on understanding the underlying electrochemistry of uranium within the electrorefiner, like Hoover's and Kim's work [7]. While all of these studies have gathered useful results regarding the performance and expected behavior for obtaining a CV measurement on an electrorefiner, further research in this area is warranted.

This study expands on prior research by using the simplified CV model developed by Phongikaroon to assess CV's ability as a whole in predicting the uranium content within the electrorefiner. This is done using realistic data obtained from a pyroprocessing flowsheet model Separation Safeguards and Performance Model, or SSPM) over a long process period (15000 hours, with one datapoint per hour) and theoretical electrorefiner data covering a range of uranium mass fractions from 0.25 wt% to 10.0 wt% (100+ datapoints). The datasets The accuracy in predicting the electrorefiner's uranium content via the CV model's output (percent difference in predicted and actual uranium content) was assessed here. Beyond this, the confidence and accuracy in the developed trends in the CV model's output versus uranium mass fraction was assessed. The influence of noise in the CV model's output (to simulate measurement noise) and impact of the amount of data used to develop these trends on this confidence was measured. The accuracy of the trends (percent difference in predicted and actual uranium content) for varying amounts of electrorefiner data and for multiple data noise values was also measured. This kind of assessment is critical for determining the performance of CV for predicting the uranium content in the electrorefiner over a wide

range of potential concentrations, and for determining how sensitive the CV results are to measurement noise and input data size.

Chapter 3

Methods

As this method is designed to operate on large sets of data, important considerations were the ease of implementation/modification, as well as the runtime for individual CV traces. While a more accurate measurement would result in more exact and physically replicable CV traces, these are likely to drastically increase runtime to where they are unusable. As such, Phongikaroon's model as described previously in the background section was adopted and modified in areas for this analysis, since it not only could be easily modified for our purposes, but also had a reasonable runtime.

The primary measurable quantity that can be obtained from a CV voltammogram is the magnitude of the difference between the cathodic and anodic peaks within the irreversible portion of the CV trace. As mentioned previously, as the potential is changed during the CV trace, oxidation and reduction reactions occur within the electrorefiner. These reactions cause large changes in the measured current, which forms two irreversible peaks: a cathodic and anodic peak. It is the difference in measured current between these two peaks that is of interest and which can be correlated with uranium concentration within the electrochemical cell. An image of an example CV-trace generated using this calculation method, with the peak difference indicated, is given in Figure 3.1 [13]. In this plot, blue indicates the reversible regions, red indicates irreversible regions, negative current indicates a cathodic region, and a positive current indicates an anodic region. The black curves are reference curves used for comparison with their model.

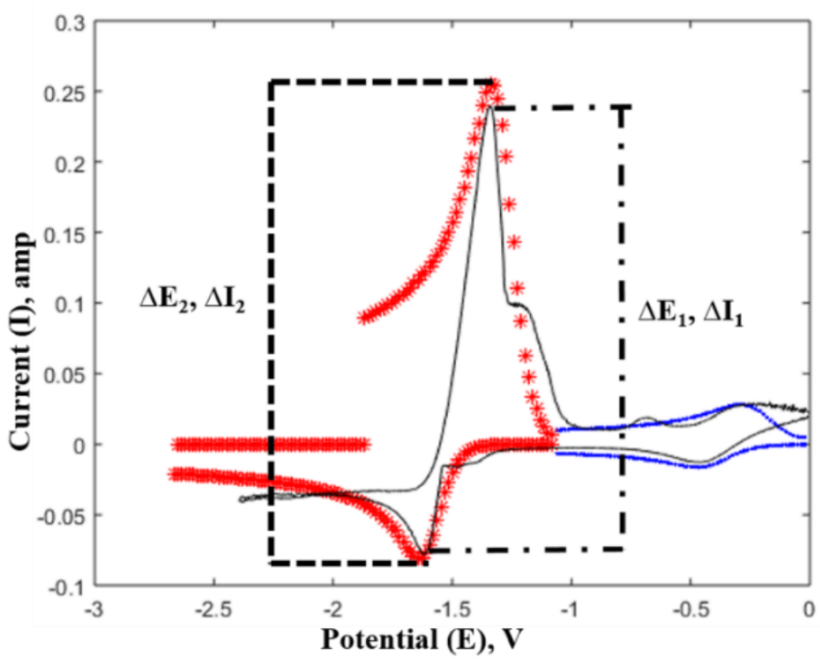


Figure 3.1: Cyclic Voltammogram for a 2.5 wt% UCl_3 solution in LiCl-KCl eutectic salt at 773 K. Data is generated using 200 $\frac{mV}{s}$ scan rate [13].

While the reference and simulated curves may differ in Figure 3.1, the magnitude of the irreversible peaks (the large, labelled peaks) is similar. This is the important aspect of the CV trace for our purposes, since it is these magnitudes (or more specifically, the magnitude of the peak difference for the two irreversible peaks) which can be correlated back to the uranium concentration in the electrorefiner. This is the reason why the model's quality is still reasonable despite the rest of the trace not correlating well with the reference.

To generate a full CV trace like the one in Figure 3.1, this model first divides the calculation into 5 separate segments. One for the cathodic reversible region (blue, bottom right), one for the cathodic irreversible region (red, bottom left), two for the anodic irreversible region (one for each half, both red on the upper left), and finally, one for the anodic reversible region (blue, upper right). In each region, data is generated point by point, starting from the right (highest potential), and using the equations provided earlier, and proceeding through the five regions in the order mentioned previously. This is how the plot in Figure 3.1 was generated.

To reiterate, it is only the irreversible peak difference that is required out of the CV measurement, since it is this quantity that can be correlated to the uranium concentration in the electrorefiner. As such, while this model is capable of generating a full-fidelity CV trace beyond the calculation of this peak difference, doing so does present inefficiencies. These inefficiencies increase the runtime of the CV module, making it less suitable for analyzing large amounts of data, such as that from SSPM. To counteract these inefficiencies, the code can be modified such that only the necessary data points are generated for finding the peak difference, reducing the computational workload and improving runtime. The first measure to accomplish this was to remove the calculations for data within the two reversible regions, as well as the data within the first half of the anodic irreversible curve. While these regions are necessary for a fully-detailed CV voltammogram, they are not involved with the calculation of the peak difference of interest here, and therefore can be safely removed.

Second, since the data in the trace is generated point by point, data generation can be halted when specified conditions are met. For our purposes, we only wish to capture the irreversible peaks (or more precisely, their magnitudes), and so to prevent excess data generation, the code was modified such that when the difference in the absolute value of the simulated current values between two consecutive data points was negative (i.e. the current began to decrease in magnitude) within a region, no further data for that region was generated. This is efficient since with this model, a current decrease always coincides with passing the irreversible peak, and as such, no further data is needed to find the peak magnitude. While this comes at the cost of not being able to generate a full CV trace for plotting, it comes with no loss of accuracy in the estimate of the peak difference, making it much more feasible to use with data from SSPM. An example plot illustrating the data generated after these two modifications were included is given in Figure 3.2.

Another issue that needed to be considered prior to utilizing this model involved which sets of input data to include. When the model is used, it requires a set of input parameters in order to develop a CV trace and extract the irreversible peak difference. These parameters include the uranium mass percent and scan rate, some physical characteristics from the system, such as the formal electrode potential in different regions of the CV trace, and diffusion coefficients for each region, and some model-specific parameters, such as the time

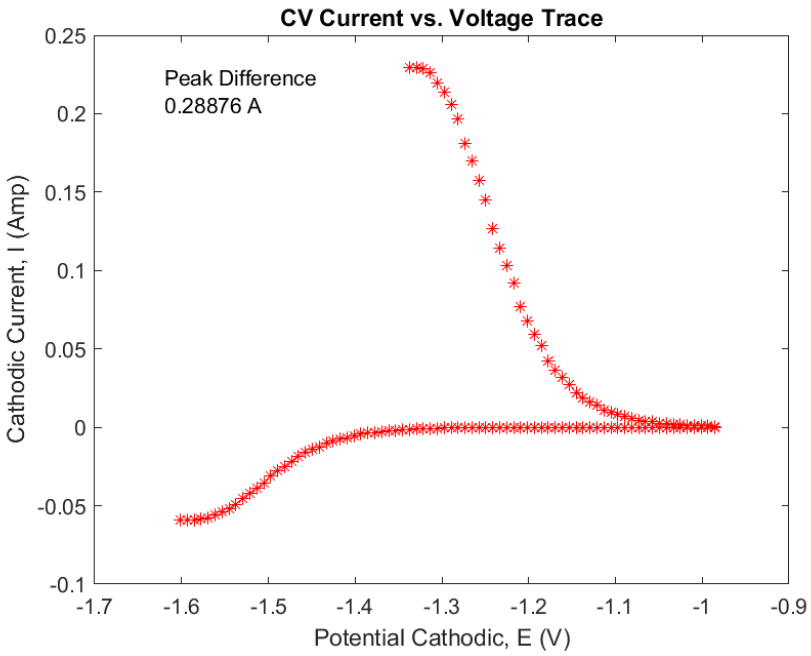


Figure 3.2: Cyclic Voltammogram for a 2.5 wt% UCl_3 solution. This illustrates how much data was cut off in order to improve efficiency during simulation run-time.

step between different datapoints within the CV trace (a full list of all the input parameters is given in Table 3.1). The original input dataset used with this model included input data that covered several different uranium concentration values (specifically, there were sets of input data for 1, 2.5, 5, 7.5 and 10 wt% uranium). For each of these discrete concentration values there were multiple sets of input data, with different scan rates and values for the remaining input parameters. However, the CV analysis implemented for this work did not require more than one set of input data for each uranium concentration, since the dependence of the irreversible peak difference on uranium concentration (versus any of the remaining parameters) was of interest here. The irreversible peaks within the CV trace do have some dependence on scan rate (namely its location within the trace), but the primary influence on the magnitude of the peak difference is the uranium concentration. As such, the original set of input data needed to be trimmed to include only a single set of input data for each uranium concentration (for a total of 5 input datasets).

Three primary concerns arose when deciding which sets of input data to include. First, since the analysis in this report involved calculating the CV peak difference at uranium

concentrations between the discrete values mentioned previously, interpolation was required for each of these input parameters based off the value of the uranium concentration. As such, ensuring that the CV peaks developed properly when the input parameters were interpolated between those values given in the trimmed set of 5 input sets was essential. Second, it was also important to ensure that trimming the input data down to 5 input datasets (one set for each uranium concentration as mentioned before) did not increase runtime via interpolation. Lastly, the influence of the uranium mass percent on the CV peak difference needed to be observable, and that the influence of no other input parameter overpowered that of uranium concentration.

From testing, it was determined that the first concern was the most prevalent. When using certain sets of input data, interpolating between them would prevent the CV peaks from appearing within the trace (which could occur, for example, from the reversible sections of the CV trace extending further than needed and covering where the peak would normally be). This issue would render the model incapable of calculating the peak difference. This rendered some of the original input datasets unusable. As for the latter two concerns, it was determined that interpolation did not significantly increase runtime (independent of which input datasets were used), and that after trimming the data down to a final set of 5 input datasets, the influence of uranium mass percent on the CV peak difference was clearly discernible, and no other input parameter overpowered its influence.

The table of 5 sets of input parameters that were found to provide usable results is given in Table 3.1. It is worth noting that the range of scan rates within this table is relatively small as compared to the original, which could have been a partial contributor to the model's stability under interpolation. This also limits the scan rate's effects on the CV trace and peak difference, leaving uranium concentration as the primary means of modifying the trace.

Finally, as some of the concentrations of uranium encountered in the electrorefiner can be very low, such as after the removal of a batch, extrapolation of input parameters for concentrations of uranium outside the bounds of the data in Table 3.1 (i.e. for uranium concentrations <1 wt%) is required for this analysis. The method by which this extrapolation was implemented was different for each input parameter. While many input parameters favored using a linear trend for extrapolation, others favored a different approach.

Table 3.1: Table of input values used for generating CV traces within SSPM. This data is used both for interpolation and extrapolation purposes between the given concentrations of uranium.

Uranium Concentration (wt%)	1.0	2.5	5.0	7.5	10.0
Scan Rate ($\frac{V}{s}$)	0.1	0.2	0.4	0.4	0.5
D(U+4/U+3) ($\frac{cm^2}{s}$)*10^5	1.05	0.7	0.45	0.45	0.2
D(U+3/U+4) ($\frac{cm^2}{s}$)*10^5	3.02	3.02	2.4	1.85	1.5
E0 Cathode Reversible (V)	-0.43	-0.43	-0.43	-0.43	-0.55
E0 Anode Reversible (V)	-0.25	-0.25	-0.25	-0.2	-0.18
D(U+3/U) ($\frac{cm^2}{s}$)*10^5	2.0	1.82	1.45	1.4	0.83
D(U/U+3) ($\frac{cm^2}{s}$)*10^5	38.0	16.5	8.5	9.5	4.4
E0 Cathode Irreversible (V)	-1.61	-1.61	-1.67	-1.7	-1.73
E0 Anode Irreversible (V)	-1.45	-1.34	-1.19	-1.09	-1.0
Initial Time (s)	0.012	0.012	0.006	0.0012	0.0012
Reversible Cathode Time (s)	9.36	3.99	2.48	1.92	1.28
Irreversible Cathode Time (s)	14.54	12.11	6.01	5.99	4.782
Irreversible Anode Time (s)	14.54	20.22	9.54	10.06	8.33
Reversible Anode Time (s)	9.34	24.22	12.02	11.97	9.59
Time Interval (s)	0.08	0.08	0.08	0.03	0.08
Area (cm^2)	0.626	0.583	0.71	0.659	0.785

The most prominent method used for the extrapolation of input parameters was linear extrapolation. Using this method, a linear trend of the parameter in question versus uranium weight percent was established over the range of data available in Table 3.1 (5 points). Using this trend, a prediction of the variable for the region of uranium concentrations below 1 wt% was used for estimating that variable's value. For most of the input variables, this extrapolation method was used. The only other method that was utilized here was simply estimating the variable as a constant for the lower mass percent region. This was used for some of the parameters for one of two reasons: The parameter remained constant within the range of the table near the 1 wt% threshold (which was the case for many of the formal electrode potentials), or because the variable did not have a direct impact on the calculation of the peak difference (which was the case for the initial time value, for example). In both of these cases, the constant value used for estimation was simply the value for the variable at 1 wt%. The exact method for extrapolation used for each variable is detailed in Table 3.2, and plots of variables using both of these extrapolation techniques are given in Figures 3.3 and 3.4.

While the formal electrode potential for the anodic irreversible portion of the CV trace (E0 Anode Irreversible in the table) exhibits linear behavior, it was kept constant in the region below 1 wt% U. This was done to keep it consistent with the method used for the formal electrode on the cathodic irreversible side (E0 Cathode Irreversible), which remained constant near the 1 wt% region. Also, the region of extrapolation is small, less than 1 wt%, so using a constant value here will not deviate much from the prediction that could be made using linear extrapolation, although a point of future study could look into the effects of using linear extrapolation for these two variables.

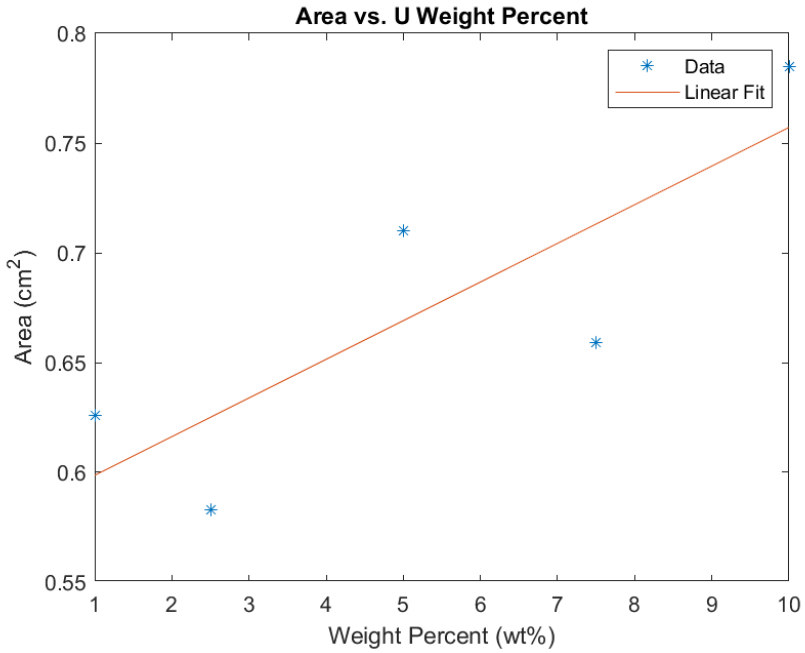


Figure 3.3: Example plot of input data suitable for a linear extrapolation into the low U wt% region. The linear trend used for such extrapolation is included for comparison with the data. This data is for the surface area at the electrode.

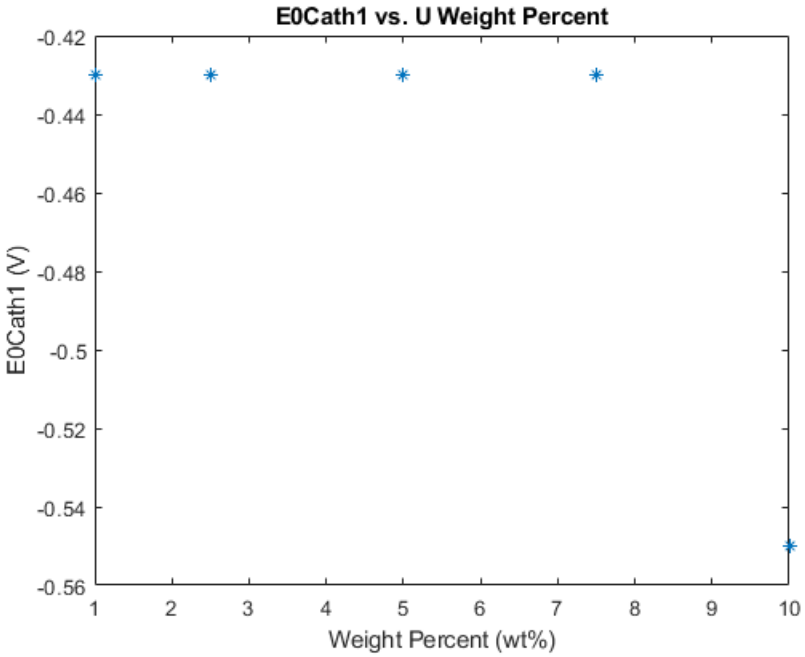


Figure 3.4: Example plot of input data suitable for a constant extrapolation into the low U wt% region. This data is for the formal electrode potential within the cathodic reversible region.

Table 3.2: List of Extrapolation Methods used for each variable in the CV input data.

Scan Rate ($\frac{V}{s}$)	Linear Extrapolation
D(U+4/U+3) ($\frac{cm^2}{s}$)*10^5	Linear Extrapolation
D(U+3/U+4) ($\frac{cm^2}{s}$)*10^5	Linear Extrapolation
E0 Cathode Reversible (V)	Constant Value
E0 Anode Reversible (V)	Constant Value
D(U+3/U) ($\frac{cm^2}{s}$)*10^5	Linear Extrapolation
D(U/U+3) ($\frac{cm^2}{s}$)*10^5	Linear Extrapolation
E0 Cathode Irreversible (V)	Constant Value
E0 Anode Irreversible (V)	Constant Value
Initial Time (s)	Constant Value
Reversible Cathode Time (s)	Linear Extrapolation
Irreversible Cathode Time (s)	Linear Extrapolation
Irreversible Anode Time (s)	Linear Extrapolation
Reversible Anode Time (s)	Linear Extrapolation
Time Interval (s)	Constant Value
Area (cm^2)	Linear Extrapolation

Chapter 4

Results

After finalizing the extrapolation procedure, the CV module was tested on sample input data generated from SSPM in order to assess the method's ability to track uranium concentration within the electrorefiner. Prior to this, the correlation between the CV peak difference and uranium weight percent was determined. To do this, a batch of input data was generated to estimate the CV peak difference over a range of uranium weight percents from 0.25 wt% to 10.0 wt%, in 0.05 wt% increments. The data of these peak differences evaluated over this range is given in Figure 4.1. To avoid confusion, input data used by the model to generate CV traces and calculate the CV peak difference will be referred to as inputs (or input data) or parameters, and output data from the CV model will be referred to as output data, data, or as the CV peak difference directly.

From what is shown in Figure 4.1, the trend between uranium weight percent and CV peak difference appears to be piecewise linear. This is to be expected, since the input data used to generate these trends is interpolated between the 5 input datasets given in Table 3.1. As such, at each of the uranium concentrations in the table (1.0, 2.5, 5.0, 7.5, and 10.0 wt%), the trend between uranium weight percent and CV peak difference should change. A plot of the trendlines for each segment versus the original data is given in Figure 4.2.

From Figure 4.2, we see that the trendlines adhere to the data effectively under most of this range. Above 7.5 wt%, the quality of the trend decreases as the data sways more from being purely linear. This was deemed acceptable, since when the SSPM simulation input

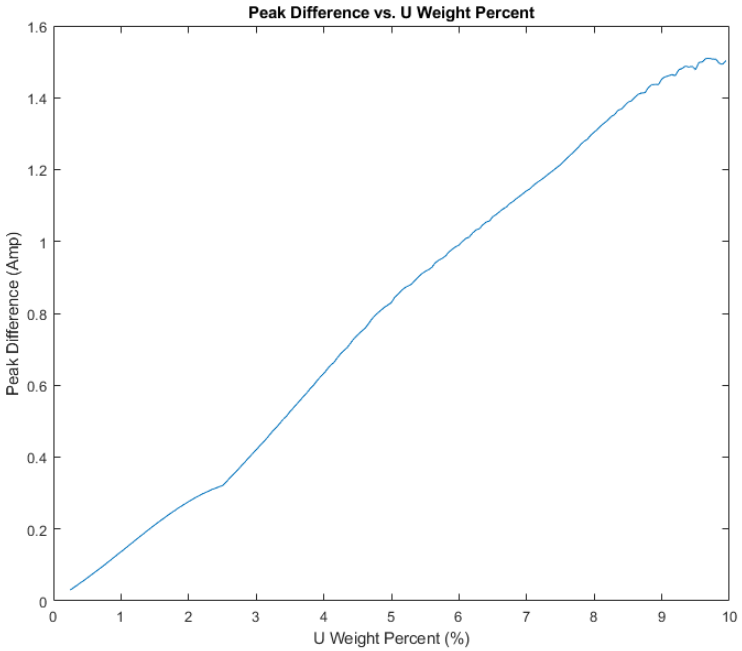


Figure 4.1: Plot of the peak current difference vs. uranium weight percent from 0.25 wt% to 10 wt%.

data was generated, the uranium weight percent within the electrorefiner never increased beyond 3 wt%, leaving only the piecewise linear data.

In addition to this, the regions for each trend (i.e. regions where the linear trend shifted) were from 0 to 2.0 wt%, from 2.0 to 2.5 wt%, from 2.5 to 5.0 wt%, from 5.0 to 7.5 wt%, and from 7.5 to 10.0 wt%. There was no shift in the trend at 1.0 wt% (meaning the extrapolated model output data for the low mass percent region had the same the same trend as the data above it), and that the trend for the 2.0 to 2.5 wt% region was different than that of the lower weight percent region. While introducing this additional region was not required, including this separate region increased the accuracy significantly. With all of the trends as described above, the largest percent difference between the data from the model and the prediction of the CV peak difference from the trend was 7.0 %, in the region above 7.5 wt%. A table of the linear trends used here are given in Table 4.1.

To assess these trends for simulated input data, a 15000 hour SSPM run was conducted to attain the uranium mass percents within the electrorefiner for a long process period. The

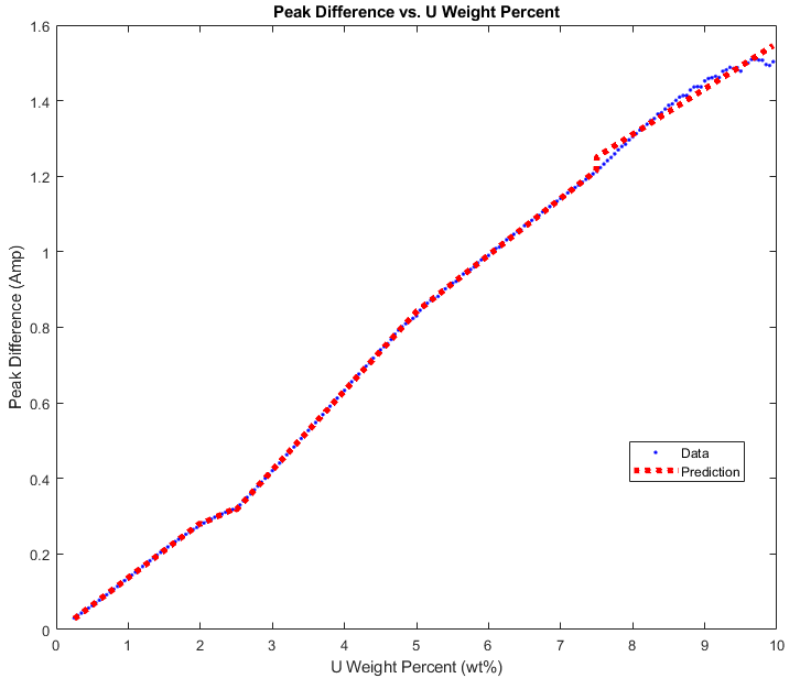


Figure 4.2: Plot of the peak current difference vs. uranium weight percent from 0.25 wt% to 10 wt%. A plot of the trendlines used in each region is used for comparison.

used fuel input into SSPM was 2.17% enriched, with a burnup of 20 GWd/MTU, and a cooling time of 5 years. A plot of the CV peak difference versus uranium weight percent for this input data is given in Figure 4.3.

From Figure 4.3, we see that the trendlines adhere to the model output data very well for this region of uranium weight percents. The largest percent difference between the model output and the predicted output from the trend was 1.97%, a significant improvement to the 7% value assessed earlier. This is expected, considering that the range of uranium weight percents used here is smaller than the previous range, and within this range, the linear trends were more accurate. Considering this, it is reasonable to expect that using the CV peak difference would be a reliable method to estimate the uranium weight percent in the electrorefiner. To further show this, the peak difference was reverse-correlated back to uranium weight percent (using the inverse relationships of the linear ones found earlier), and this predicted weight percent was plotted versus time and compared to the actual weight

Table 4.1: Linear Trends used for Correlating CV Peak Difference and Uranium Weight Percent.

Region	Slope (A/wt%)	Intercept (A)
<2.0 wt%	0.1449	-0.0079
2.0 to 2.5 wt%	0.0860	0.1070
2.5 to 5.0 wt%	0.2099	-0.2078
5.0 to 7.5 wt%	0.1497	0.0929
>7.5 wt%	0.1205	0.3469

percent. This plot is shown in Figure 4.4 for hours 1 to 1000 (time was limited for ease of inspection).

Figure 4.4 depicts the uranium content of the electrorefiner over several drawdown periods. From the figure, we see that the uranium content was well-tracked via the predictions from the trends previously established in the CV output. Over the course of the whole 15000 hour process period, the maximum percent difference between the predicted and actual uranium weight percent within the electrorefiner was 1.90%, indicating further that CV, when implemented properly, could serve as an effective measure of uranium content.

Beyond these error calculations, a few other measures were evaluated in order to get a more clear sense of the accuracy of the calculated trends. In particular, the influence of noise in the output data (not noise in any of the input parameters for the model), and the size of the dataset (i.e. how many different uranium mass percent values were used when evaluating trends) on the trends' quality was evaluated. This kind of analysis would be important to consider for calibration of a CV measurement device, as the correlations between the CV peak difference and uranium concentration would be used to back-calculate the uranium content in the electrorefiner, as was done here. To simulate noise, first output model data was again generated over the range of 0.25 wt% to 10.0 wt% uranium using the same methods as before, with a specified number of data points (i.e. uranium mass percent-CV peak difference value pairs). From here, at each data point, the peak difference was recalculated around this mean value from the model to simulate noise. This extra noise for the output data was implemented by assuming a normal distribution for the noise profile, so the peak difference was sampled from a normal distribution with a mean value equal to

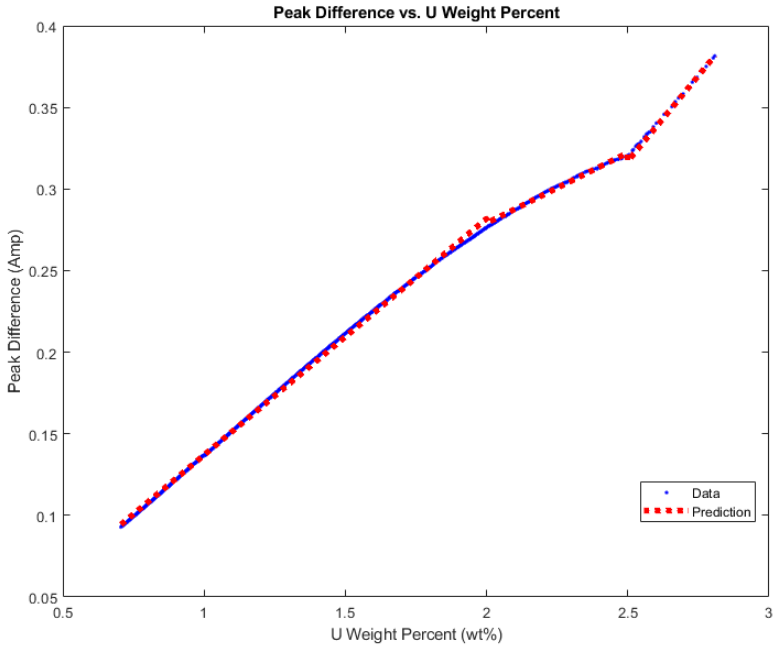


Figure 4.3: Plot of the CV peak difference vs. uranium weight percent for the range of data calculated with a 15000 hour SSPM. The fuel input had a cooling time of 5 years, was 2.17% enriched, and had a burnup of 20 GWd/MTU. Trendlines are included for comparison.

the CV peak difference from the model, and with varying values for the standard deviation. Once this noise was implemented for all of the output data, the piecewise linear fits for each region were re-evaluated.

This procedure was implemented multiple times, to get a set of calculated linear trends for each region, using different noisy data for each one (but with the same mean CV peak difference and same standard deviation in the noise). From this set of trends, the uncertainty in the each of the regions' slope and intercept values was evaluated (by calculating the standard deviation of the respective trend value) to get a measure of the spread in the trend values. Sets of noisy output data for calculating trends this way were generated until the standard deviation value converged for each slope and intercept value (<1% change in standard deviation value from including trend values from an additional dataset). This not only allows us to assess the confidence in each trend, but also allows for comparisons in the trend distributions between regions.

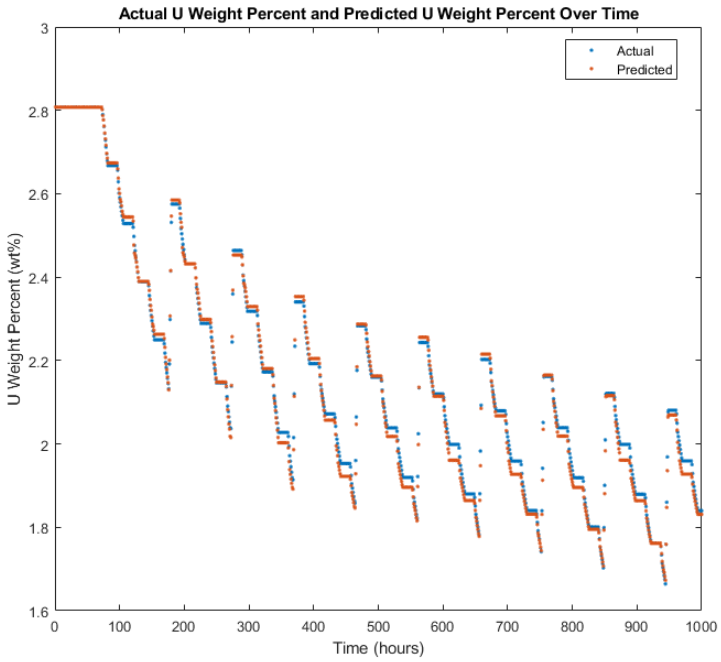


Figure 4.4: Plot of the predicted and actual uranium weight percent over time. From this, we see that the predictions mach closely with the actual content within the electrorefiner.

The influence of the number of data points on the trends was done by doing the same procedure as just described, but with a different number of data points. Multiple values for the number of data points as well as the magnitude of the data noise were included to assess their impact on the trend. To assess the impact of data noise, 5%, 10%, and 15% noise values (these were values for the standard deviation in the noise) were used to get a good spread in the magnitude of the noise. As for the amount of data, this was varied by changing the increment at which data was evaluated via the model. Before, to determine the correlations, 0.05 wt% increments in the uranium mass fraction were used (roughly 200 data points). Here, 0.1 wt% (roughly 100 data points), 0.05 wt%, and 0.02 wt% (roughly 500 data points) increments were used, to discern how having different amounts of data changed the spread of slope and intercept values within each region. The major results of this analysis will be presented here, with the remaining data being included in the appendix.

It is important to note before continuing that this noise added into the data is artificial, and is done in addition to any systematic errors the model itself produces (simply from how

it calculates data and its assumptions). As a result, with larger relative uncertainties, the accuracy of prediction decreases significantly. However, this amount of error, compounded with the model error, is not expected to be present in an actual system. That being said, the influence of noise in the data is an important consideration to be made since noise will always be present within any physical system, and so this analysis is still included here.

First, the influence on the number of data points was investigated. Tables 4.2 and 4.3 show the mean slopes and intercepts for each region, with their associated uncertainties, using a 5% noise in each data point while varying the number of data points from 100 to 500. From these two tables, we clearly see the influence of the calibration data size on the uncertainty, with the larger data size reducing the uncertainty by roughly 50%. While for larger regions, such as the first and third regions, this uncertainty difference will not be as significant, for the second region, a much larger magnitude difference was observed. This is because for the trends evaluated using 100 data points, only a few pieces of data remained within this region, but using 500 points, many more points were contained here, allowing for significantly increased confidence in the trend values.

Table 4.2: Slopes, Intercepts, and Associated Uncertainties for Each Region Using 100 Points With 5% Data Noise.

Region	Mean Slope (A/wt%)	Uncertainty (A/wt%)	Mean Intercept (A)	Uncertainty (A)
<2 wt%	0.1442	0.0035	-0.0074	0.0030
2 to 2.5 wt%	0.0767	0.0614	0.1303	0.1411
2.5 to 5 wt%	0.2096	0.0097	-0.2064	0.0359
5 to 7.5 wt%	0.1510	0.0165	0.0857	0.1035
7.5 to 10 wt%	0.1200	0.0211	0.3527	0.1855

Table 4.3: Slopes, Intercepts, and Associated Uncertainties for Each Region Using 500 Points With 5% Data Noise.

Region	Mean Slope (A/wt%)	Uncertainty (A/wt%)	Mean Intercept (A)	Uncertainty (A)
<2 wt%	0.1448	0.0019	-0.0078	0.0015
2 to 2.5 wt%	0.0870	0.0231	0.1049	0.0526
2.5 to 5 wt%	0.2099	0.0036	-0.2078	0.0128
5 to 7.5 wt%	0.1493	0.0080	0.0961	0.0491
7.5 to 10 wt%	0.1236	0.0079	0.3187	0.0689

These findings have important implications for any CV modules integrated into a pyroprocessing plant. Most importantly, it is essential that calibration data used to evaluate trends like these cover the entire span of expected operating conditions within the electrorefiner: that is, if the plant is expecting the uranium weight percent within the electrorefiner to be within a certain range, the calibration data must cover that region, and there must be enough data points in the calibration data for said region in order to develop trends with reasonable accuracy. If, for example, a plant expected the electrorefiner to operate near 2 wt% uranium, then many data points near here would be needed to calibrate the device, and using the same data density as used for Table 4.2 would almost certainly be insufficient. Exactly just how many data points can be included in the calibration data will depend on the plant (for example, how much time is allotted for calibration, and how finely you can manipulate the uranium content during calibration measurements will both influence the calibration data size), but the data's influence on the confidence in the trends should not be overlooked.

Next, the noise in the data points was considered. Tables 4.4 and 4.5 consider the cases where 200 data points were used to evaluate trends, but with 5% and 15% noise in the data respectively. From these two tables, we can see that with increased data error, there is vastly increased uncertainty in the slope and intercept for each evaluated trend. This is especially true for the second region, where the smaller amount of data points led to large trend uncertainties for the 15% data noise case. Based off this, we see that these correlations are sensitive to the noise in the data. This would mean that for devices more prone to measurement error, additional procedures (such as adding more datapoints, as discussed earlier) to reduce its impact would be required. Overall, the influences from adding extra datapoints into the calibration set and changing the noise in the data are as expected: including more data reduced the uncertainty in the evaluated trends, and increasing data noise significantly increased this uncertainty.

Next, the z-scores for each trend were evaluated, so that the z-score of the slope could be plotted against the z-score of the intercept for each calculated trend. This was implemented using a 200 data points and 5% data noise (since the results were identical for each data size-data noise combination from before). This analysis was done to get a more visual

Table 4.4: Slopes, Intercepts, and Associated Uncertainties for Each Region Using 200 Points With 5% Data Error.

Region	Mean Slope (A/wt%)	Uncertainty (A/wt%)	Mean Intercept (A)	Uncertainty (A)
<2 wt%	0.1449	0.0031	-0.0078	0.0026
2 to 2.5 wt%	0.0869	0.0347	0.1059	0.0789
2.5 to 5 wt%	0.2105	0.0063	-.2099	0.0221
5 to 7.5 wt%	0.1505	0.0082	0.0902	0.0521
7.5 to 10 wt%	0.1190	0.0130	0.3614	0.1164

Table 4.5: Slopes, Intercepts, and Associated Uncertainties for Each Region Using 200 Points With 15% Data Error.

Region	Mean Slope (A/wt%)	Uncertainty (A/wt%)	Mean Intercept (A)	Uncertainty (A)
<2 wt%	0.1447	0.0108	-0.0074	0.0089
2 to 2.5 wt%	0.0968	0.0809	0.0794	0.1807
2.5 to 5 wt%	0.2099	0.0181	-0.2077	0.0665
5 to 7.5 wt%	0.1438	0.0302	0.1227	0.1871
7.5 to 10 wt%	0.1182	0.0453	0.3702	0.3961

representation of the spread of the trend values, and to ensure the shape or spread of the distributions of the slope and intercept values did not change significantly between regions. The z-scores for each of these slope and intercept values were calculated using equation 4.1, where Z is the z-score, x is a slope or intercept value for a particular noisy output dataset, $\bar{x}$ is the mean value for that slope or intercept value over multiple noisy output datasets, and σ_x is the standard deviation of that slope or intercept value over multiple noisy output datasets.

$$Z = \frac{x - \bar{x}}{\sigma_x} \tag{4.1}$$

This z-score data was calculated for each region, and was graphed in Figures 4.5 and 4.6 as a scatterplot and heat map respectively (for the heat map, more noisy output data sets were generated so that the spread was more visible.) From the two plots, we can discern a few important features. First, the distributions, after being normalized this way, is similar for each region. The first region containing small uranium concentrations does exhibit a

degree of additional spread in the slope, but other than this discrepancy, the regions are otherwise very similar. This means that the individual trends evaluated in each region had roughly the same distribution shape, and that no region in particular displayed unusual behavior in their shape. However, while the normalized z-score distributions are very similar, some regions (like the second one) do exhibit more spread in the non-normalized case, since the uncertainty in the evaluated trends is higher there. Figure 4.5 only confirms that the shape of each distribution is similar, not the magnitude to which each region's trendlines are distributed from the mean.

The other important note to make from these plots is that the correlation between slope z-score and intercept z-score is negative and linear. This indicates that a poor-quality value for one portion of the fit will yield a bad value for the other portion, just on the opposite side of the mean. This emphasizes further the importance of collecting enough calibration data, as getting a bad fit would yield poor predictions of the uranium content in the electrorefiner down the road. Collecting multiple sets of calibration data would yield to more confidence in the trend (less uncertainty), and mitigate the possibility of a single outlier dataset of compromising the accuracy of the CV device.

Lastly, for each combination of data size (100, 200, and 500 points) and data noise magnitude (5%, 10%, and 15%), multiple sets of noisy output data were generated as done previously. For each generated set of noisy output data, the CV peak difference was correlated back to uranium weight percent, and the difference between the correlated and actual uranium weight percent values was calculated. The average (mean) percent difference and maximum percent difference over the full range of uranium weight percent values was determined, and the process was repeated again several times. The average of these two percent difference values (that is, the average of both quantities over multiple sets of noisy output data) was then calculated in order to get a sense of the accuracy of back-correlating from these trends when data uncertainty is included (this was similar to what was done with the data from SSPM, instead here it is with multiple datasets, over a larger range of uranium content, and includes random noise in the data). The results of these calculations are included in Tables 4.6 and 4.7.

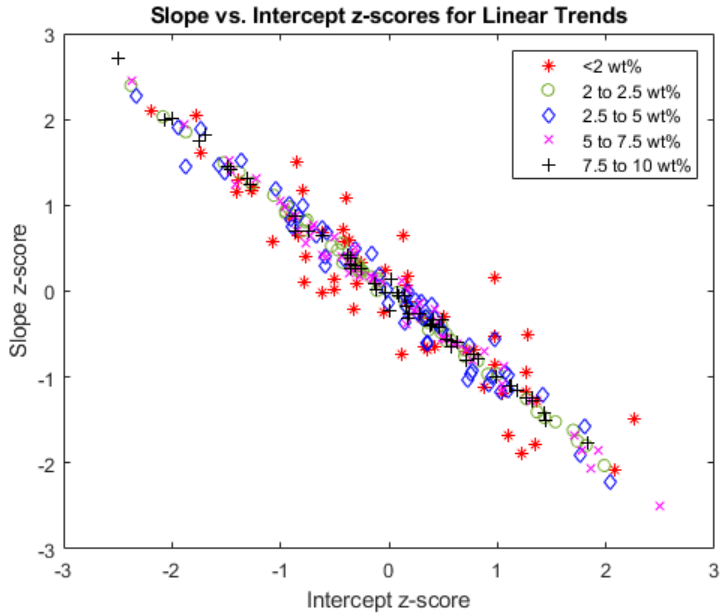


Figure 4.5: Plot of z-scores for slope and intercept values for each region. The spreads look very similar after being normalized here, but considering that each region has different standard deviations for their individual slopes and intercepts, we know that the regions with high uncertainties in their measured trends exhibit much more spread, despite having the same shape as the rest.

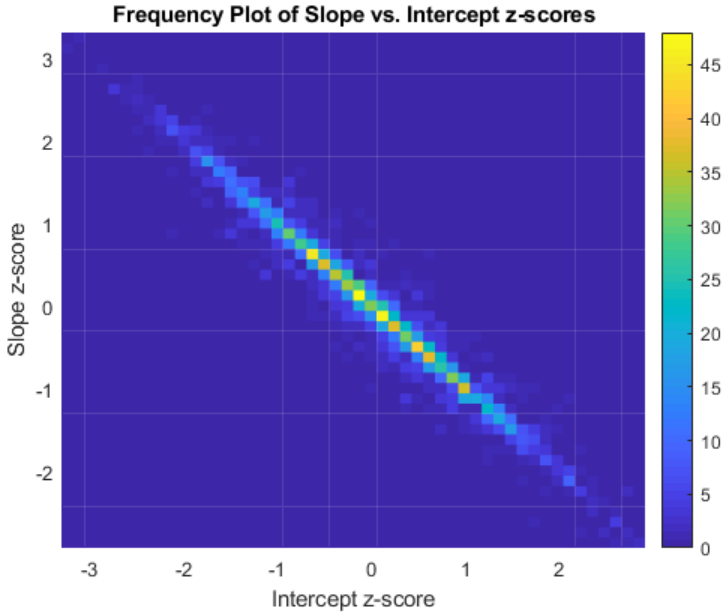


Figure 4.6: Plot of z-scores for slope and intercept values for each region as a heat map.

Table 4.6: Mean Error in Prediction of Uranium Weight Percent for Different Data Noise Values and Data Sizes Over the Range of 0.25 wt% to 10.0 wt%.

# Data Points	No Added Noise	5% Data Noise	10% Data Noise	15% Data Noise
100	0.67%	3.76%	6.29%	8.22%
200	0.67%	3.74%	6.26%	8.19%
500	0.67%	3.74%	6.31%	8.27%

Table 4.7: Average Maximum Error in Prediction of Uranium Weight Percent for Different Data Noise Values and Data Sizes Over the Range of 0.25 wt% to 10.0 wt%.

# Data Points	No Added Noise	5% Data Noise	10% Data Noise	15% Data Noise
100	6.02%	14.92%	27.76%	43.29%
200	6.02%	15.01%	27.26%	44.56%
500	5.84%	15.98%	30.02%	53.77%

From these two tables, we see that adding additional output datapoints did not significantly affect either accuracy measure, but increasing the noise in the data significantly affected both the mean accuracy and maximum error measurements. In the case of the maximum error, differences between the correlated and actual uranium weight percents approached nearly 50%. The influence of data uncertainty on the trends indicates two important notions regarding the use of cyclic voltammetry. First, when implementing this measurement in the pyroprocessing system, it is essential that any artificial biases in the measurement be mitigated or removed, otherwise they will introduce significant data noise and result in much worse accuracy as shown here. Second, since removing all noise in the data is impossible, it is important to remember that cyclic voltammetry is not intended as the only means of measuring uranium content in the electrorefiner. Instead, it is intended to be a part of a larger material accountancy/safeguards system for the plant. This way, the failure of a single measurement technique will not lead towards a failure in maintaining an accurate measure of uranium content.

It might be discerned from these tables that including additional points in the calibration dataset when analyzing trends is not necessary, as doing so does not increase the mean accuracy. This is a false interpretation of the data, as the measures of accuracy were done

by averaging the two respective quantities in Tables 4.6 and 4.7 over many sets of noisy data, rather than just using a single one. The influence of including additional data points has the added benefit of reducing the uncertainty in slope and intercept values for each region, and therefore mitigates the chance of a measured trend in the data being an outlier and leading to more unstable predictions of uranium content. Having fewer datapoints on the other hand increases this chance, and is therefore undesirable.

Chapter 5

Summary and Future Work

The results of this assessment of cyclic voltammetry (CV) show that the technique is promising for the purpose of material accountancy and safeguards within a prospective pyroprocessing facility. When piecewise linear correlations between the uranium weight percent and the simulated CV irreversible peak difference were assessed over the range of uranium weight percent values of 0.25 wt% to 10.0 wt%, it was found that the actual simulated peak difference matched up well with the peak difference predicted by the trends, with a maximum percent difference of roughly 7%. Results improved further when a dataset produced from the pyroprocessing flowsheet SSPM were analyzed. Here, the maximum percent difference between the predicted and actual peak difference decreased to only 1.97%. Both of these results indicate that the peak difference output from a CV measurement are linearly correlated with uranium weight percent. To further show this, the previously evaluated trendlines were used to reverse-correlate the CV output with the uranium weight percent. When this was done for the same set of SSPM data, the maximum percent difference between the predicted and actual uranium content in the electrorefiner lied at only 1.90%, showing that the method is capable of predicting the amount of uranium in the vessel efficiently if implemented correctly.

Next, the dependence of the evaluated trends on noise in the data and the size of the dataset was assessed. Using a dataset size of 200, when going from 5% to 15% noise in the data, uncertainties in the slope and intercept values found for the trendlines nearly tripled. Similarly, when using data with 5% relative noise, decreasing the data size from 500 points

to only 100 points increased the uncertainties in each trend by 100% or more. These results both show that data noise and data size have a significant effect on the accuracy of the evaluated trends. Knowing this, in a physical setting, it is important to limit or elimininate the effects of any biases it may have when acquiring data, and when calibrating the device, it is essential to not only have an adequately sized dataset, but to also have data that covers the expected range of uranium weight percents in the electrorefiner. Having additional data within the expected region of operation will greatly improve results and mitigate the possibility of erroneous predictions due to a poorly optimized fit

When considering the error in the trends used to reverse-correlate the uranium concentration from the CV output (with data noise), it was discovered that while the dataset size did not have a significant impact on the performance of the individual correlations on average, the magnitude of the data uncertainty did. This once again emphasizes the point of mitigating any systematic and random error when performing a CV scan. In addition, although the size of the dataset on average did not influence the average or maximum error over the range of the data, increasing the dataset size still does have its benefits in that there is less spread in the possible slope and intercept values, as shown before. This means that there is a smaller likelihood for an observed trend during calibration to deviate far from the actual trend, thus reducing the chances of erroneously reporting the uranium concentration in the electrorefiner.

Overall, CV shows promising results for predicting uranium content within the electrorefiner, but it is critical that any evaluated trends found via CV be obtained properly and carefully. The data used to calibrate and evaluate trends needs to be large enough to minimize spread in the possible slope and intercept values, needs to cover the expected range of uranium concentration within the electrorefiner for the specific facility, and the influence of any biases present within the data itself needs to be minimized, either by reducing systematic/random error directly, or by taking the same data multiple times to get more accurate averaged results. If done properly however, CV results correlate very well with uranium concentration, and can be used to monitor the content within the electrorefiner for safeguards or material accountancy purposes if bundled in as part of a larger system with the same accountancy and safeguards purposes.

Future work in this area would involve obtaining and analyzing more potential datasets which measure the concentration of uranium in the electrorefiner. This would necessitate the inclusion of a wider set of input data by which the model could use to simulate peak differences. Performing this analysis would allow for the assessment of the method over a wider range of uranium concentrations, which could be beneficial depending on the operating conditions of the plant. Other important work that could be done would be to analyze the uncertainties in the input data that the model uses, and assess their influence on the result. This would be useful in discerning which input data parameters have the most influence on the output, making it easier to find efficient ways of reducing the influence of uncertainties in the input data and provide motivation for research into minimizing error on any of the input parameters.

While this model can develop a CV trace for a uranium system, it does not include the influence of any additional elements within the fuel. Hoover mentioned in his study that significant quantities of zirconium within the electrorefiner could significantly impact the CV trace, and warrant different methods by which to attain the peak current from uranium [3]. This influence from other elements within the electrorefiner would likely increase the uncertainty in the evaluated peak current from uranium, and was not characterized in this study. Future studies could look further into this impact by adding additional fidelity to the model to include the influence of different elements and performing a similar analysis, or by performing the CV measurements on a physical system. Such analysis would require electrorefiner data to cover a wide range of uranium concentrations and any other elements' concentrations which could impact the CV trace.

Additionally, it is currently unknown whether a calibration for correlating the output of a CV measurement to uranium concentration would require a different correlation per pyroprocessing plant or whether a general correlation could be used for all plants. To assess this, future studies would need to investigate the impact of different physical characteristics of the electrorefiner on the CV trace, such as different eutectic salts (aside from just LiCl-KCl), different operating temperatures, or the inclusion or exclusion of a liquid cathode for plutonium withdrawal. The significance of each of these physical characteristics would then need to be assessed over a wide array of fuel inputs to quantify their influence on

the prediction of uranium content. This kind of study would be able to determine which characteristics influence the CV trace the most and whether different correlations for different electrorefiner designs or operating conditions would be warranted.

Bibliography

[1] Chang, Y. I., Benedict, R. W., Bucknor, M. D., Figueroa, J., Herceg, J. E., Johnson, T. R., Koehl, E. R., Lell, R. M., Park, Y. S., Pope, C. L., Wiedmeyer, S. G., Williamson, M. A., Willit, J. L., James, R., Meyers, S., Spaulding, B., Underdahl, J., and Wolf, M. (2018). Conceptual design of a pilot-scale pyroprocessing facility. *Nuclear Technology*, 205(5):708–726. xi, 3, 4, 5

[2] Coble, J., Skutnik, S., Gilliam, S. N., Cooper, M., and Mitchell, J. (2020). Integrating data sources for improved safeguards and accountancy of electrochemical fuel reprocessing systems. Technical report, University of Tennessee, Knoxville. 2

[3] Hoover, R. O. (2014). *Uranium and Zirconium Electrochemical Studies in LiCl-KCl Eutectic for Fundamental Applications in Used Nuclear Fuel Reprocessing.* PhD thesis, University of Idaho. xi, 7, 8, 9, 11, 37

[4] IAEA (2001). Iaea safeguards glossary, 2001 edition. ix, 5, 6

[5] Johnson, C. W., Dunzik-Gougar, M. L., and Li, S. X. (2006). On-line Monitoring of Actinide Concentrations in Molten Salt Electrolyte. In *Transactions of the American Nuclear Society*, volume 95(1), pages 129–130. INL/CON-06-11515. 9

[6] Karell, E. J., Gourishankar, K. V., Smith, J. L., Chow, L. S., and Redey, L. (2001). Separation of actinides from lwr spent fuel using molten-salt-based electrochemical processes. *Nuclear Technology*, 136(3):342–353. 4

[7] Kim, T.-J., Jung, Y., Shim, J.-B., Kim, S.-H., Paek, S., Kim, K.-R., Ahn, D.-H., and Lee, H. (2011). Study on physicochemical properties of u3+ in licl–kcl eutectic media at 773 k. *Journal of Radioanalytical and Nuclear Chemistry*, 287(1):347–350. 10, 11

[8] Lafreniere, P. L., Rappleye, D. S., Hoover, R. O., Simpson, M. F., and Blandford, E. D. (2015). Demonstration of signature-based safeguards for pyroprocessing as applied to electrorefining and the ingot casting process. *Nuclear Technology*, 189(2):173–185. 5

[9] Laidler, J., Battles, J., Miller, W., Ackerman, J., and Carls, E. (1997). Development of pyroprocessing technology. *Progress in Nuclear Energy*, 31(1-2):131–140. 4

[10] Lee, H., Park, G.-I., Lee, J.-W., Kang, K.-H., Hur, J.-M., Kim, J.-G., Paek, S., Kim, I.-T., and Cho, I.-J. (2013). Current status of pyroprocessing development at kaeri. *Science and Technology of Nuclear Installations*, 2013:11. 4

[11] Nicholson, R. S. and Shain, I. (1964). Theory of stationary electrode polarography. single scan and cyclic methods applied to reversible, irreversible, and kinetic systems. *Analytical Chemistry*, 36(4):706–723. 8

[12] Pouri, S. and Phongikaroon, S. (2017). An interactive reverse-engineering cyclic voltammetry for uranium electrochemical studies in licl-kcl eutectic salt. 7, 8, 10

[13] Pouri, S. R. (2017). *Comparative Studies of Diffusion Models and Artificial Neural Intelligence on Electrochemical Process of U and Zr Dissolutions in LiCl-KCl Eutectic Salts*. PhD thesis, Virginia Commonwealth University. xi, 7, 8, 10, 11, 13, 14, 54

[14] Pouri, S. R. and Phongikaroon, S. (2016). Graphical user interface with reverse-engineering of the cyclic voltammetry method for electrochemmical processes of used nuclear fuel. 8

[15] Rakhshan Pouri, S., Manic, M., and Phongikaroon, S. (2018). A novel framework for intelligent signal detection via artificial neural networks for cyclic voltammetry in pyroprocessing technology. *Annals of nuclear energy*, 111:242–254. 10

[16] Rappleye, D., Newton, M. L., Zhang, C., and Simpson, M. F. (2017). Electroanalytical measurements of binary-analyte mixtures in molten licl-kcl eutectic: Uranium(iii)- and magnesium(ii)-chloride. *Journal of Nuclear Materials*, 486(C):369–380. 10

[17] Riley, T., Pope, C., and Benedict, R. (2016). Safeguards performance model for evaluation of potential safeguards strategies applied to pyroprocessing facilities. *Nuclear engineering and design*, 301:157–163. 4

[18] Simpson, M. F. (2012). Developments of spent nuclear fuel pyroprocessing technology at idaho national laboratory. 3, 4

[19] Yoo, J.-H., Seo, C.-S., Kim, E.-H., and Lee, H.-S. (2008). A conceptual study of pyroprocessing for recovering actinides from spent oxide fuels. *Nuclear Engineering and Technology*, 40(7):581–592. 3

Appendices

A Miscellaneous Figures

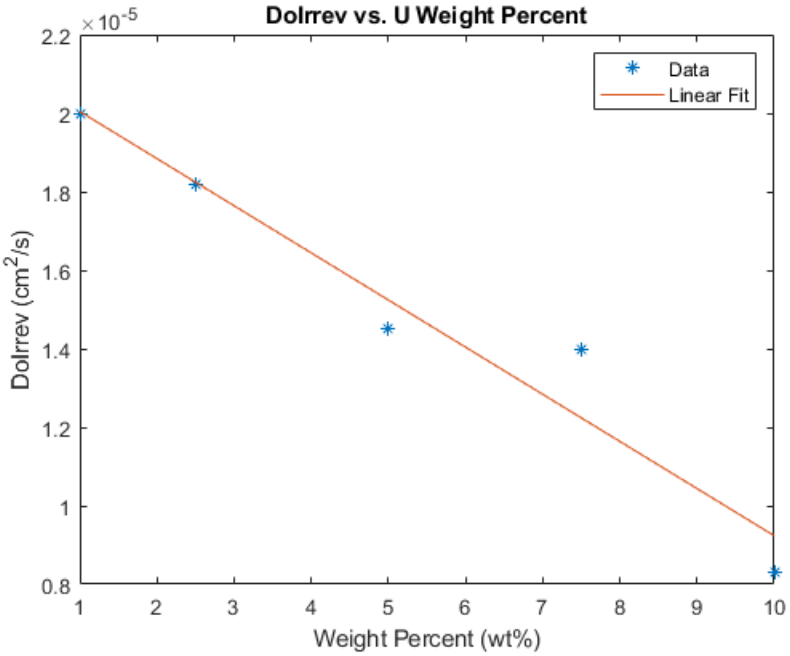


Figure A.1: Example plot of data suitable for a linear extrapolation into the low U wt% region. The linear trend used for such extrapolation is included for comparison with the data. This data is for the diffusion coefficient of the oxidized species on the irreversible side.

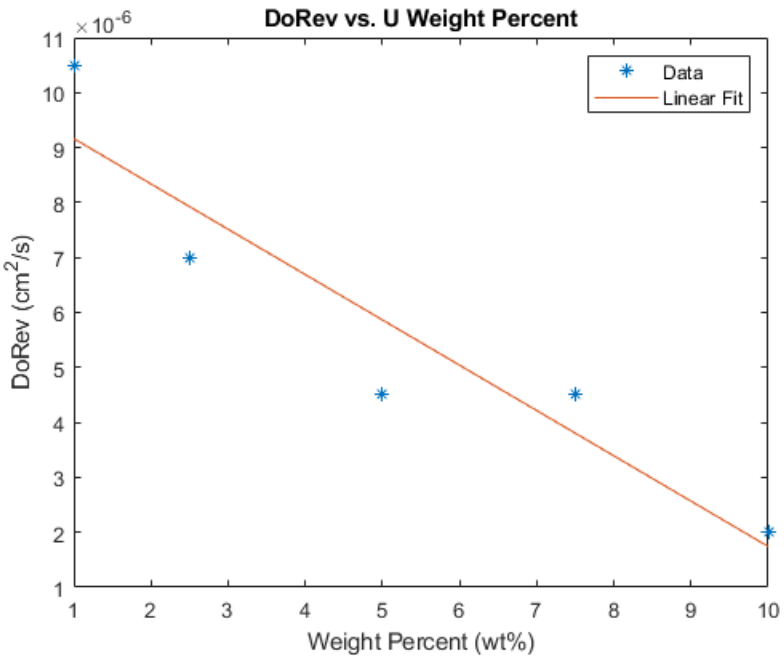


Figure A.2: Example plot of data suitable for a linear extrapolation into the low U wt% region. The linear trend used for such extrapolation is included for comparison with the data. This data is for the diffusion coefficient of the oxidized species on the reversible side.

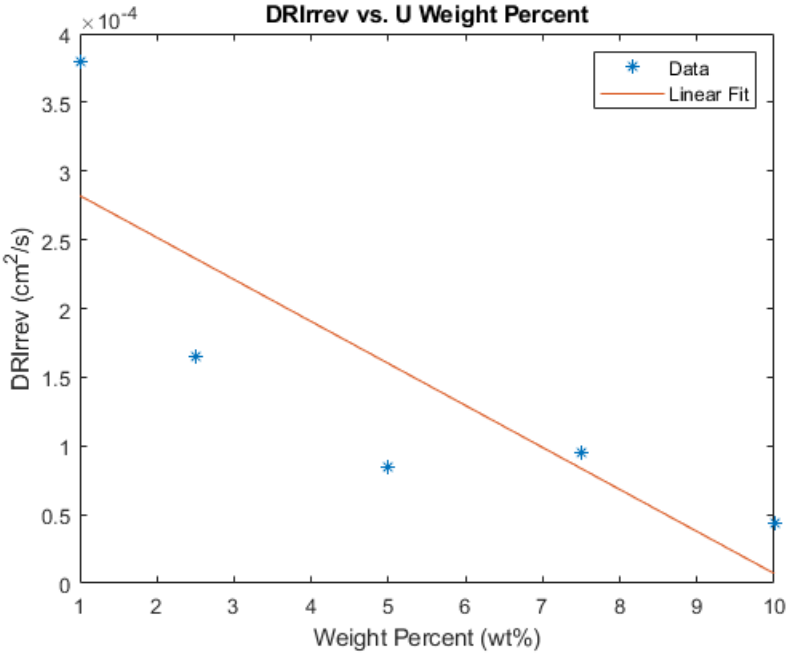


Figure A.3: Example plot of data suitable for a linear extrapolation into the low U wt% region. The linear trend used for such extrapolation is included for comparison with the data. This data is for the diffusion coefficient of the reduced species on the irreversible side.

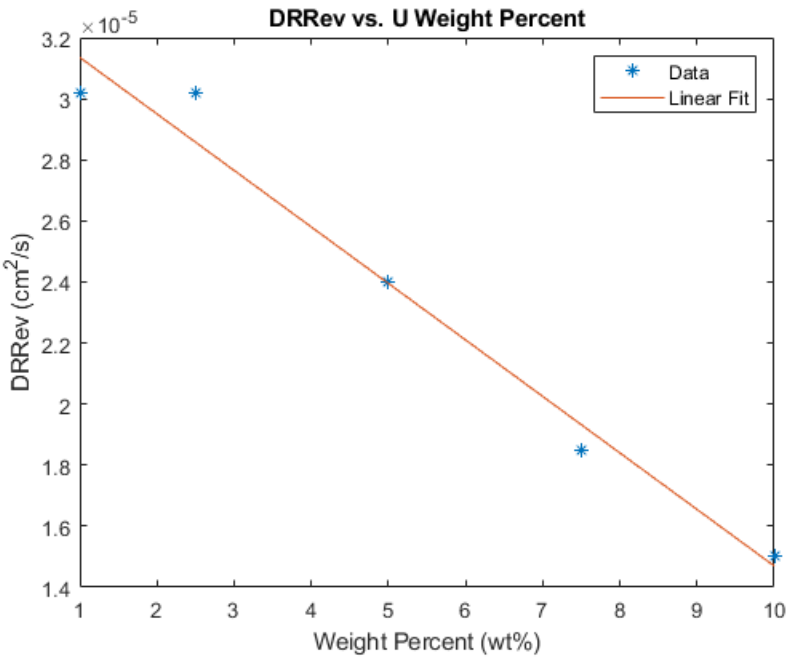


Figure A.4: Example plot of data suitable for a linear extrapolation into the low U wt% region. The linear trend used for such extrapolation is included for comparison with the data. This data is for the diffusion coefficient of the reduced species on the reversible side.

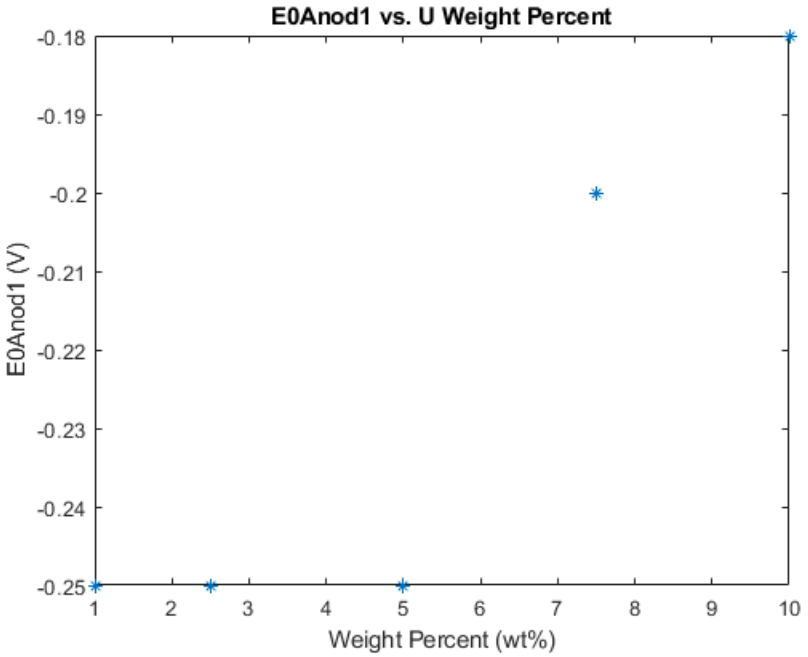


Figure A.5: Example plot of data suitable for a linear extrapolation into the low U wt% region. The linear trend used for such extrapolation is included for comparison with the data. This data is for the formal electrode potential on the anodic reversible side.

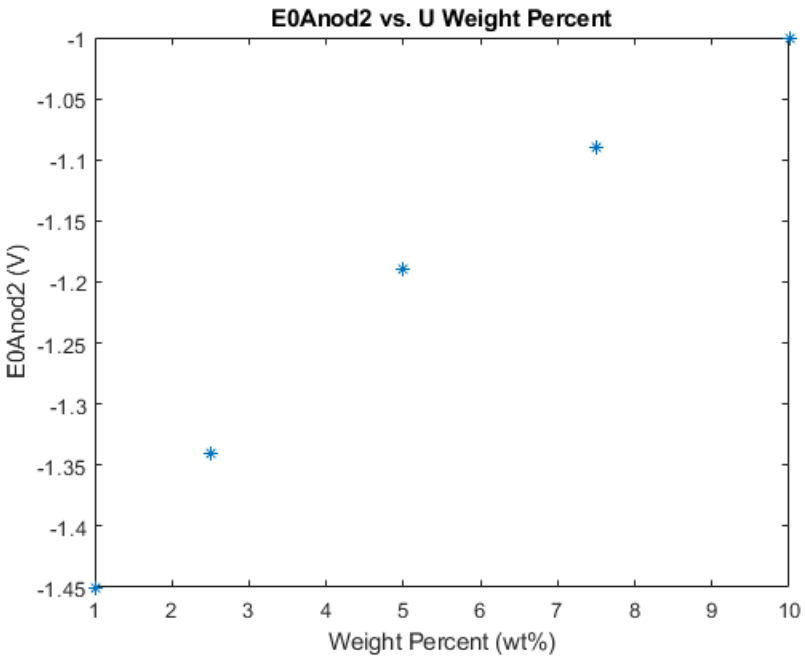


Figure A.6: Example plot of data suitable for a linear extrapolation into the low U wt% region. The linear trend used for such extrapolation is included for comparison with the data. This data is for the formal electrode potential on the anodic irreversible side.

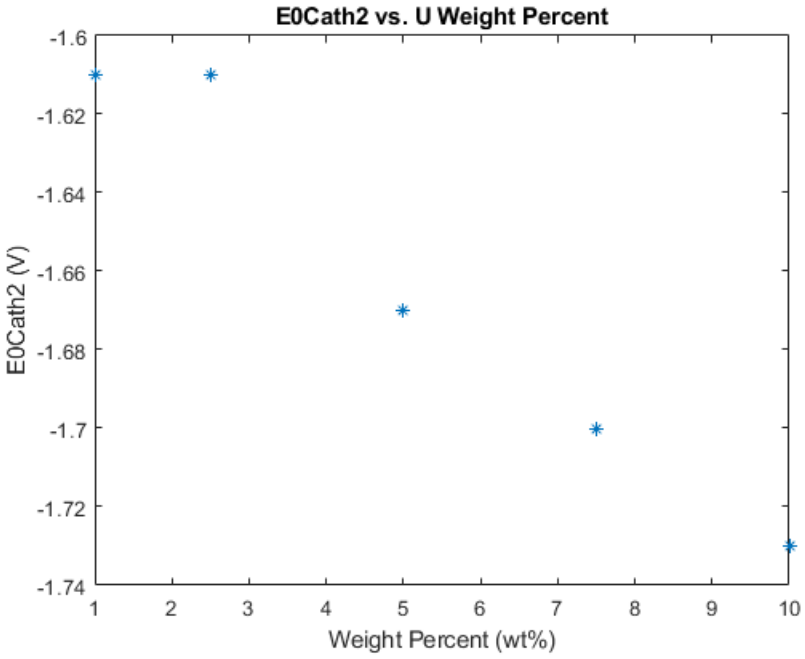


Figure A.7: Example plot of data suitable for a linear extrapolation into the low U wt% region. The linear trend used for such extrapolation is included for comparison with the data. This data is for the formal electrode potential on the cathodic irreversible side.

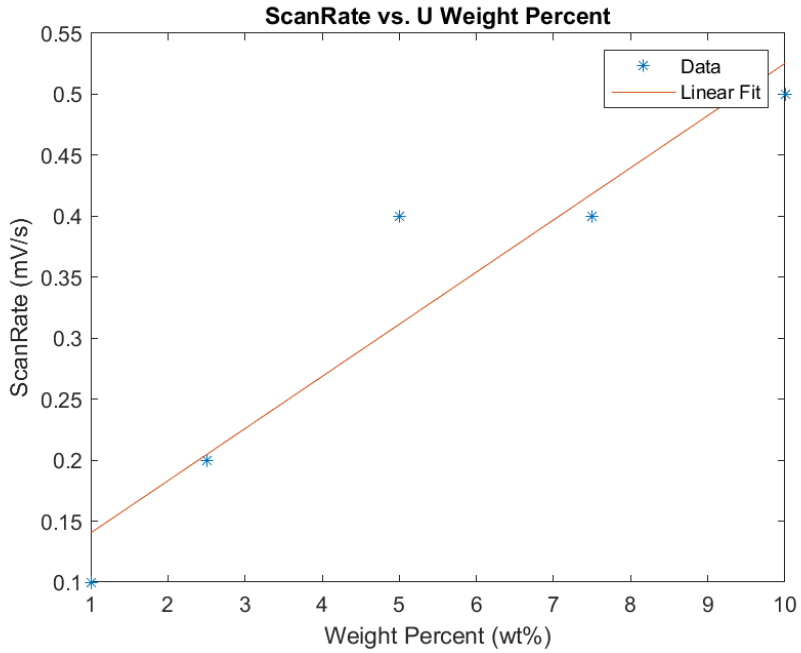


Figure A.8: Example plot of data suitable for a linear extrapolation into the low U wt% region. The linear trend used for such extrapolation is included for comparison with the data. This data is for the scan rate.

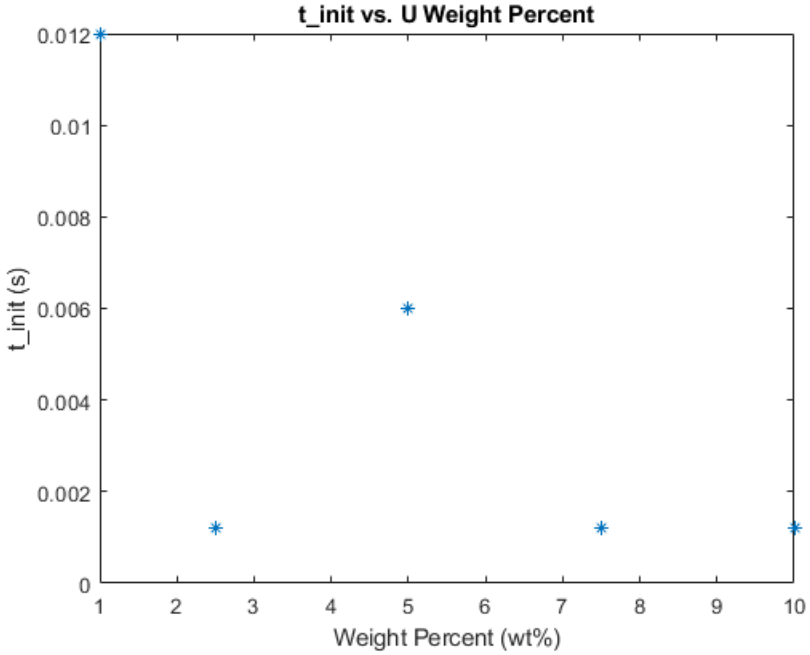


Figure A.9: Example plot of data suitable for a linear extrapolation into the low U wt% region. The linear trend used for such extrapolation is included for comparison with the data. This data is for the initial time.

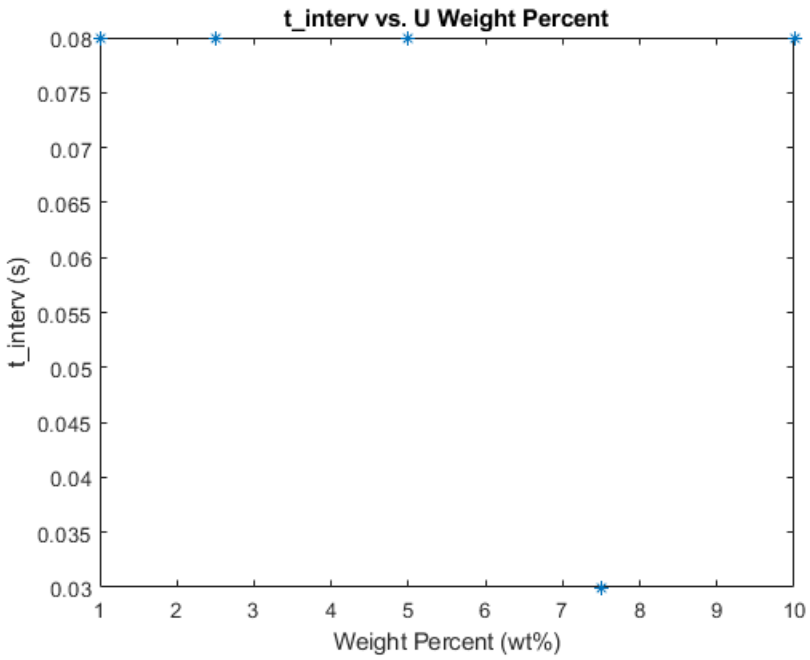


Figure A.10: Example plot of data suitable for a linear extrapolation into the low U wt% region. The linear trend used for such extrapolation is included for comparison with the data. This data is for the time interval between points on the CV scan.

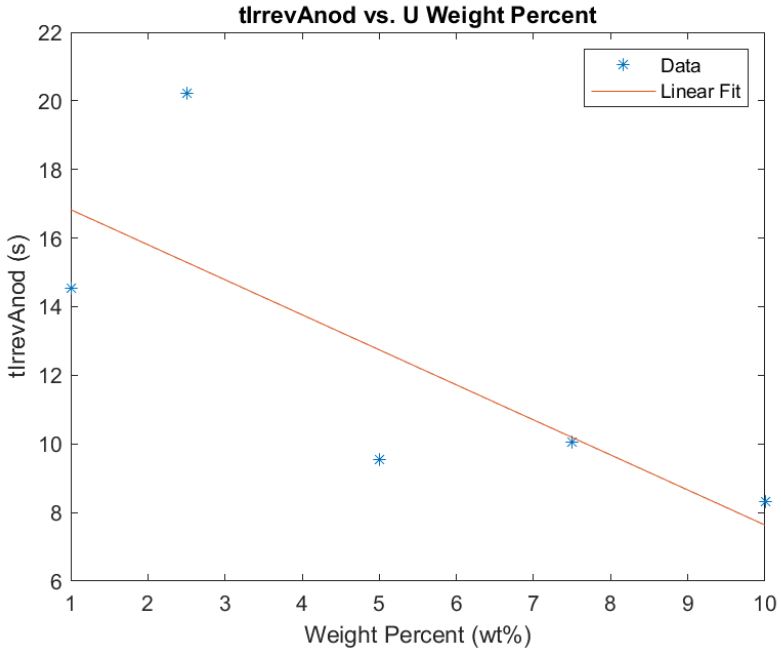


Figure A.11: Example plot of data suitable for a linear extrapolation into the low U wt% region. The linear trend used for such extrapolation is included for comparison with the data. This data is for the time spent on the anodic irreversible side.

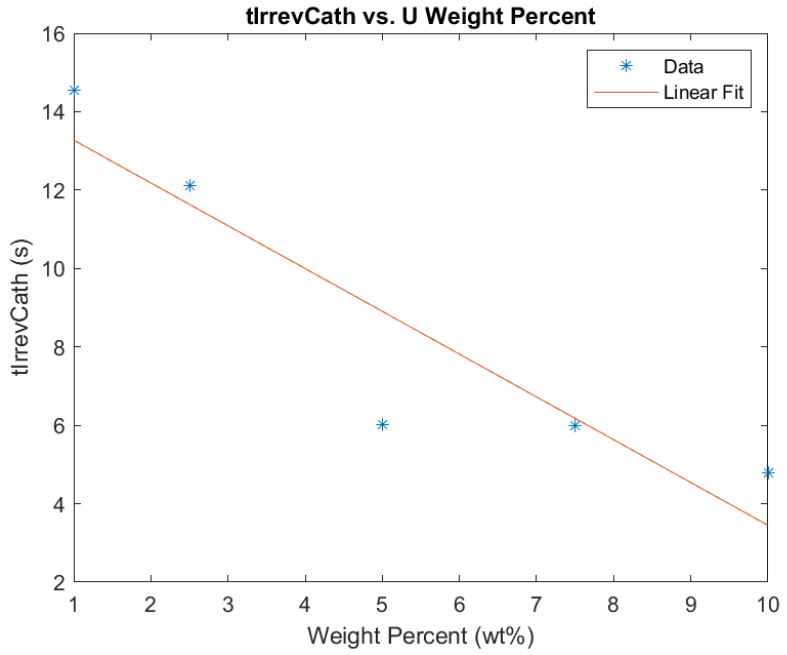


Figure A.12: Example plot of data suitable for a linear extrapolation into the low U wt% region. The linear trend used for such extrapolation is included for comparison with the data. This data is for the time spent on the cathodic irreversible side.

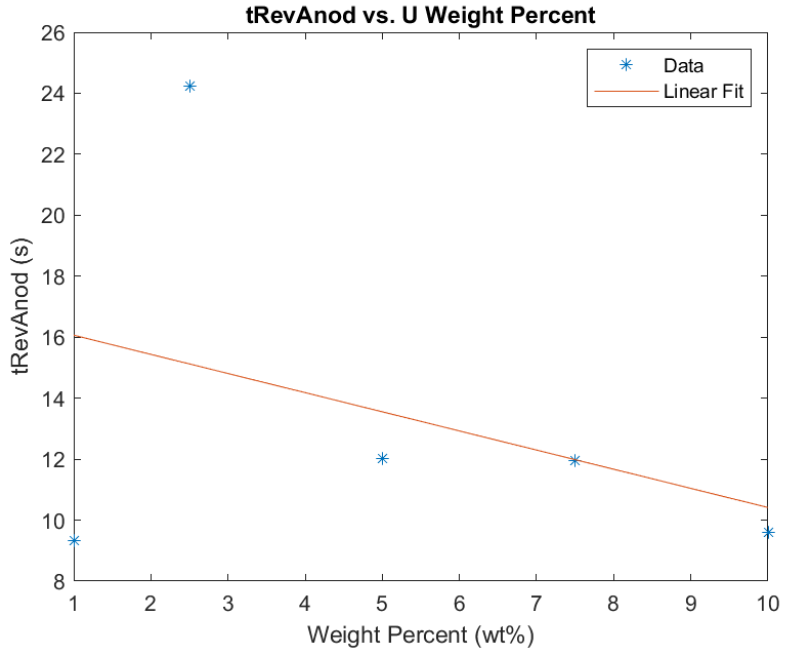


Figure A.13: Example plot of data suitable for a linear extrapolation into the low U wt% region. The linear trend used for such extrapolation is included for comparison with the data. This data is for the time spent on the anodic reversible side.

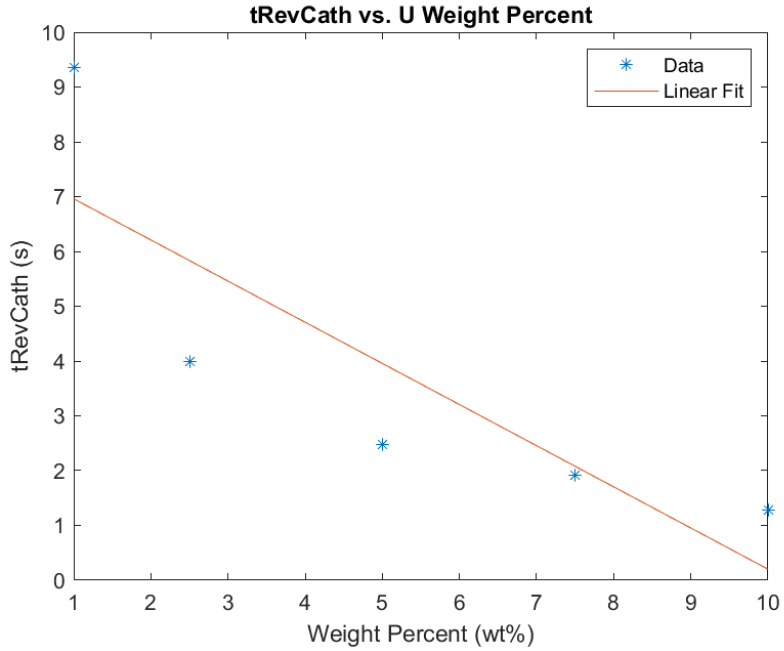


Figure A.14: Example plot of data suitable for a linear extrapolation into the low U wt% region. The linear trend used for such extrapolation is included for comparison with the data. This data is for the time spent on the cathodic reversible side.

B Miscellaneous Tables

Table B.1: Slopes, Intercepts, and Associated Uncertainties for Each Region Using 100 Points With 10% Data Noise.

Region	Mean Slope (A/wt%)	Uncertainty (A/wt%)	Mean Intercept (A)	Uncertainty (A)
<2 wt%	0.1455	0.0081	-0.0082	0.0066
2 to 2.5 wt%	0.0903	0.1341	0.0977	0.3076
2.5 to 5 wt%	0.2098	0.0181	-0.2080	0.0644
5 to 7.5 wt%	0.1499	0.0298	0.0911	0.1854
7.5 to 10 wt%	0.1182	0.0388	0.3670	0.3399

Table B.2: Slopes, Intercepts, and Associated Uncertainties for Each Region Using 100 Points With 15% Data Noise.

Region	Mean Slope (A/wt%)	Uncertainty (A/wt%)	Mean Intercept (A)	Uncertainty (A)
<2 wt%	0.1456	0.0124	-0.0083	0.0102
2 to 2.5 wt%	0.0837	0.1985	0.1119	0.4557
2.5 to 5 wt%	0.2106	0.0278	-0.2107	0.0982
5 to 7.5 wt%	0.1508	0.0493	0.0869	0.3065
7.5 to 10 wt%	0.1183	0.0629	0.3656	0.5477

Table B.3: Slopes, Intercepts, and Associated Uncertainties for Each Region Using 200 Points With 10% Data Noise.

Region	Mean Slope (A/wt%)	Uncertainty (A/wt%)	Mean Intercept (A)	Uncertainty (A)
<2 wt%	0.1446	0.0059	-0.0077	0.0049
2 to 2.5 wt%	0.0917	0.0650	0.0940	0.1471
2.5 to 5 wt%	0.2099	0.0127	-0.2074	0.0449
5 to 7.5 wt%	0.1506	0.0215	0.0863	0.1322
7.5 to 10 wt%	0.1216	0.0302	0.3394	0.2630

Table B.4: Slopes, Intercepts, and Associated Uncertainties for Each Region Using 500 Points With 10% Data Noise.

Region	Mean Slope (A/wt%)	Uncertainty (A/wt%)	Mean Intercept (A)	Uncertainty (A)
<2 wt%	0.1446	0.0040	-0.0077	0.0033
2 to 2.5 wt%	0.0870	0.0449	0.1047	0.1016
2.5 to 5 wt%	0.2097	0.0076	-0.2065	0.0259
5 to 7.5 wt%	0.1502	0.0133	0.0902	0.0817
7.5 to 10 wt%	0.1217	0.0173	0.3355	0.1498

Table B.5: Slopes, Intercepts, and Associated Uncertainties for Each Region Using 500 Points With 15% Data Noise.

Region	Mean Slope (A/wt%)	Uncertainty (A/wt%)	Mean Intercept (A)	Uncertainty (A)
<2 wt%	0.1448	0.0057	-0.0079	0.0048
2 to 2.5 wt%	0.0897	0.0664	0.0990	0.1501
2.5 to 5 wt%	0.2095	0.0107	-0.2067	0.0376
5 to 7.5 wt%	0.1496	0.0198	0.0934	0.1214
7.5 to 10 wt%	0.1226	0.0257	0.3266	0.2243

C MATLAB Codes

This is a compilation of all of the additional MATLAB codes used for this report. The model used in this analysis was adapted from the model used in [13].

C.1 Initialize_CV_Data.m

```
%This function is just used to initialize some parameters later
    used in the
%model, and is executed prior to performing calculations.

%1 refers to reversible regions, 2 refers to irreversible

WeightPerc_Data = [1.00,1.00,1.00,2.50,2.50,2.50,2.50,5.00,...
    5.00,5.00,5.00,7.50,7.50,7.50,7.50,7.50,10.00,10.00,10.00];

ScanRate_Data = [100.0,150.0,200.0,100.0,150.0,200.0,300.0,...
    400.0,600.0,900.0,1000.0,400.0,500.0,1000.0,1400.0,...
    2000.0,200.0,500.0,800.0]/1000;

DoRev_Data = [1.05,1.05,1.05,0.70,0.70,0.70,1.05,0.45,0.45,...
    0.45,0.45,0.45,0.49,0.50,0.50,0.50,0.25,0.20,0.13]*10^-5;

DRRev_Data = [3.02,3.02,3.02,3.02,2.70,3.02,3.02,2.40,2.40,...
    2.40,2.40,1.85,1.85,2.2,2.2,2.45,0.75,1.50,1.8]*10^-5;

E0Cath1_Data =
   [-0.43,-0.43,-0.43,-0.43,-0.43,-0.43,-0.43,-0.43,...
    -0.43,-0.43,-0.43,-0.43,-0.43,-0.5,-0.5,-0.5,-0.4,-0.55,-0.55];
```

```
E0Anod1_Data =
   [-0.25,-0.25,-0.25,-0.25,-0.25,-0.25,-0.25,-0.25,-0.25,...
    -0.23,-0.23,-0.2,-0.2,-0.16,-0.16,-0.145,-0.18,-0.18,-0.18];


DoIrrev_Data = [2.0,2.0,2.0,2.0,2.0,1.82,1.75,1.45,1.5,...
    1.18,1.18,1.4,1.4,1.05,0.99,0.94,0.93,0.83,0.65]*10^-5;

DRIrrev_Data = [3.8,2.9,2.5,3.0,2.15,1.65,1.3,0.85,0.7,...
    0.53,0.52,0.95,0.75,0.5,0.418,0.34,0.9,0.44,0.3]*10^-4;

E0Cath2_Data =
   [-1.61,-1.61,-1.61,-1.6,-1.6,-1.61,-1.62,-1.67,...
    -1.67,-1.67,-1.7,-1.7,-1.7,-1.75,-1.79,-1.81,-1.68,-1.73,-1.75];


E0Anod2_Data = [-1.45,-1.42,-1.41,-1.34,-1.34,-1.34,-1.32,...
    -1.19,-1.16,-1.13,-1.13,-1.09,-1.07,-0.98,-0.94,-0.88,-1.05,...

    -1.00,-0.95];

t_init_Data = [12,12,12,1.2,1.2,1.2,1.2,6,6,4,4,1.2,1.2,1.2,...
    1.2,1.2,1.2,1.2,1.2]*10^-3;

tRevCath_Data = [9.36,6.62,4.76,9.74,6.67,3.99,3.16,2.48,...
    1.64,0.96,0.81,1.92,1.33,0.65,0.494,0.34,3.65,1.28,0.85];

tIrrevCath_Data = [14.54,15.83,12.08,24.05,16.0,12.11,8.0,...
    6.01,3.98,2.66,2.39,5.99,4.74,2.39,1.72,1.195,11.98,...
    4.792,2.991];
```

```
tIrrevAnod_Data = [14.54,25.03,19.40,38.35,25.33,20.22,...
    12.84,9.54,6.32,4.37,3.98,10.06,8.16,4.13,2.95,2.051,...
    20.94,8.33,5.14];

tRevAnod_Data = [9.34,31.65,24.15,48.09,32.00,24.22,16.00,...
    12.02,7.95,5.32,4.79,11.97,9.48,4.79,3.45,2.39,23.98,9.59,5.98];


t_interv_Data = [0.08,0.08,0.08,0.08,0.08,0.08,0.08,0.08,...
    0.04,0.04,0.04,0.03,0.03,0.02,0.02,0.02,0.08,0.08,0.05];

Area_Data =
   [0.626,0.626,0.626,0.583,0.583,0.583,0.583,0.710,...
    0.710,0.710,0.710,0.659,0.659,0.659,0.659,0.659,0.785,0.785,0.785];


CV_Data = [WeightPerc_Data
           ScanRate_Data
           DoRev_Data
           DRRev_Data
           E0Cath1_Data
           E0Anod1_Data
           DoIrrev_Data
           DRIrrev_Data
           E0Cath2_Data
           E0Anod2_Data
           t_init_Data
           tRevCath_Data
           tIrrevCath_Data
```

```
            tIrrevAnod_Data
            tRevAnod_Data
            t_interv_Data
            Area_Data];

F = 96485;
T = 773.15;
R = 8.314;
Ei = -0.003297064;
ks = 0.00026;
Alpha = 0.5;
M_UCl3 = 344.39;

Rho_melt_LiCl = 1.502;
Rho_melt_KCl = 1.527;
T_melt_LiCl = 610;
T_melt_KCl = 771;
k_LiCl= 0.000432;
k_KCl = 0.000583;
Rho_LiCl = Rho_melt_LiCl - (k_LiCl*((T-273.15)-T_melt_LiCl));
Rho_KCl = Rho_melt_KCl - (k_KCl*((T-273.15)-T_melt_KCl));
Rho = 0.5*(Rho_LiCl + Rho_KCl);

Fit_Eqs = [0,0;
            0.0427767354596623,   0.0975609756097561;
           -8.24577861163227e-07, 9.98780487804878e-06;
           -1.85046904315197e-06, 3.32024390243902e-05;
           -0.0108067542213884,  -0.397804878048780;
            0.00846153846153845, -0.270000000000000;
           -1.20075046904315e-06, 2.12439024390244e-05;
```

```
            -3.05590994371482e-05,  0.000312707317073171;
            -0.0144652908067542,   -1.58878048780488;
             0.0495121951219512,   -1.47146341463415;
            -0.000869043151969982,  0.00883902439024390;
            -0.750863039399625,     7.71048780487805;
            -1.09171482176360,      14.3653170731707;
            -1.02153846153846,      17.8500000000000;
            -0.627823639774859,     16.6926829268293;
            -0.00215759849906191,   0.0812195121951219;
             0.0176060037523452,    0.581048780487805];

%Data_OLD =
   [1.00,1.00,1.00,2.50,2.50,2.50,2.50,5.00,5.00,5.00,5.00;
%
   100.0,150.0,200.0,100.0,150.0,200.0,300.0,400.0,600.0,900.0,1000.0;

%         1.05,1.05,1.05,0.7,0.7,0.7,1.05,0.45,0.45,0.45,0.45;
%         3.02,3.02,3.02,3.02,2.7,3.02,3.02,2.4,2.4,2.4,2.4;
%
   -0.43,-0.43,-0.43,-0.43,-0.43,-0.43,-0.43,-0.43,-0.43,-0.43,-0.43;

%
   -0.25,-0.25,-0.25,-0.25,-0.25,-0.25,-0.25,-0.25,-0.25,-0.23,-0.23;

%         2.0,2.0,2.0,2.0,2.0,1.82,1.75,1.45,1.50,1.18,1.18;
%
   3.80,2.90,2.50,3.00,2.15,1.65,1.30,0.85,0.70,0.53,0.52;
%
   -1.61,-1.61,-1.61,-1.6,-1.6,-1.61,-1.62,-1.67,-1.67,-1.7,-1.7;
```

```
%
   -1.45,-1.42,-1.41,-1.34,-1.34,-1.34,-1.32,-1.19,-1.16,-1.13,-1.13;

%         12.0,12.0,12.0,1.2,1.2,1.2,1.2,6.0,6.0,4.0,4.0;
%
   9.36,6.62,4.76,9.74,6.67,3.99,3.16,2.48,1.64,0.96,0.81;
%
   14.54,15.83,12.08,24.05,16.0,12.11,8.0,6.01,3.98,2.66,2.39;
%
   14.54,25.03,19.40,38.35,25.33,20.22,12.84,9.54,6.32,4.37,3.98;

%
   9.34,31.65,24.15,48.09,32.00,24.22,16.00,12.02,7.95,5.32,4.79;

%         0.08,0.08,0.08,0.08,0.08,0.08,0.08,0.08,0.04,0.04,0.04
%       ];
```

C.2 Trim_Data.m

```
%This function trims down the larger array of data down to data
    that just
%includes one set of input parameters per uranium concentration
   . This is
%done so that the primary influence on the CV output is the
   uranium content
%versus any other variable.

Use_Indices = [1,6,8,12,18];

WeightPerc_Data = WeightPerc_Data(Use_Indices);
```

```
ScanRate_Data = ScanRate_Data(Use_Indices);
DoRev_Data = DoRev_Data(Use_Indices);
DRRev_Data = DRRev_Data(Use_Indices);
E0Cath1_Data = E0Cath1_Data(Use_Indices);
E0Anod1_Data = E0Anod1_Data(Use_Indices);
DoIrrev_Data = DoIrrev_Data(Use_Indices);
DRIrrev_Data = DRIrrev_Data(Use_Indices);
E0Cath2_Data = E0Cath2_Data(Use_Indices);
E0Anod2_Data = E0Anod2_Data(Use_Indices);
t_init_Data = t_init_Data(Use_Indices);
tRevCath_Data = tRevCath_Data(Use_Indices);
tIrrevCath_Data = tIrrevCath_Data(Use_Indices);
tIrrevAnod_Data = tIrrevAnod_Data(Use_Indices);
tRevAnod_Data = tRevAnod_Data(Use_Indices);
t_interv_Data = t_interv_Data(Use_Indices);
Area_Data = Area_Data(Use_Indices);
CV_Data = CV_Data(:,Use_Indices);
```

C.3 CV_Data_Select.m

```
%This is the module which selects a set of input data to run
   through the
%model based off of the uranium weight percent. It does
   interpolation
%between uranium concentrations given in the data, and
   extrapolates below 1
%wt% using the extrapolation methods discussed in the methods
   section of
%the report.
```

```
if exist('WgtVec','var') > 0
    %Calculates the uranium wt% from the given data.
    Wt_Select = 100*WgtVec(92)/sum(WgtVec);
    %This condition indicates extrapolation below 1 wt%
    if Wt_Select <= min(WeightPerc_Data)
        disp('Warning! Outside of bounds of experimental data')
           ;
        Data_Select = CV_Data(:,1);
        %Performs constant extrapolation for some variables,
           and linear
        %extrapolation for the rest.
        for k = 2:size(CV_Data,1)
            if k == 5 || k == 6 || k == 9 || k == 10 || k == 11
                continue
            end
            Data_Select(k) = polyval(Fit_Eqs(k,:),Wt_Select);
        end
        Data_Select(1) = Wt_Select;
    %This condiction indicates extrapolation above 10 wt%.
       Constant
    %extrapolation is used in this case, although no
       calculations were
    %performed above this threshold.
    elseif Wt_Select >= max(WeightPerc_Data)
        disp('Warning! Outside of bounds of experimental data')
           ;
        Data_Select = CV_Data(:,end);
        Data_Select(1) = Wt_Select;
    else
```

```
        %Finds Wt% in data immediately below and above the
           selected value
        Wt_Below = WeightPerc_Data(find(WeightPerc_Data <=
           Wt_Select,1,'last'));
        Wt_Above = WeightPerc_Data(find(WeightPerc_Data >
           Wt_Select,1));
        %Finds Index (column) values in data immediately lower
        %and above the selected value
        Index_Below = find(WeightPerc_Data == Wt_Below);
        Index_Above = find(WeightPerc_Data == Wt_Above);
        %Finds mean of data of same weight percent as
           previously found,
        %both above and below the target uranium wt%
        mean_Below = mean(CV_Data(:,Index_Below),2);
        mean_Above = mean(CV_Data(:,Index_Above),2);
        %Calculates mean of data above and below target uranium
            wt%
        mean_In = [mean_Below(1),mean_Above(1)];
        mean_Out = [mean_Below(2:end),mean_Above(2:end)]';
        %Interpolates this data
        Select_Out = interp1(mean_In,mean_Out,Wt_Select)';
        Data_Select = [Wt_Select;Select_Out];
        %Data_Select = mean_Below + (mean_Above-mean_Below)...
        %*(Wt_Select-Wt_Below)/(Wt_Above-Wt_Below);
        Data_Select(1) = Wt_Select;
    end
elseif exist('Index','var') > 0 && Index >= 1 && Index <=
   length(WeightPerc_Data)
    Data_Select = CV_Data(:,Index);
end
```

```
Wt = Data_Select(1);
ScanRate = Data_Select(2);
DoRev = Data_Select(3);
DRRev = Data_Select(4);
E0Cath1 = Data_Select(5);
E0Anod1 = Data_Select(6);
DoIrrev = Data_Select(7);
DRIrrev = Data_Select(8);
E0Cath2 = Data_Select(9);
E0Anod2 = Data_Select(10);
t_init = Data_Select(11);
tRevCath = Data_Select(12);
tIrrevCath = Data_Select(13);
tIrrevAnod = Data_Select(14);
tRevAnod = Data_Select(15);
t_interv = Data_Select(16);
Area = Data_Select(17);
```

C.4 SweepTest.m

```
%This simply makes a plot of the CV peak current difference vs.
    uranium
%concentration over a specified range. By default, this range
   is from 0.25
% wt% to 10 wt%, since is the total range of the data (
   including some
% extrapolation below 1 wt%).

Wgt = 0.25;
```

```
Wgt_Increment = 0.02;
Length_Vec = round(1 + (10-0.25)/(Wgt_Increment));
Peak_Diff_Vec = zeros(Length_Vec,1);
Scan_Rate_Vec = zeros(Length_Vec,1);
U_Wt_Vec = zeros(Length_Vec,1);
Wgt_Iter = 1;

%Iterates through each desired uranium weight percent and
   calculates the CV
%peak difference for each one.
while Wgt_Iter <= Length_Vec
    WgtVec = zeros(100,1);
    WgtVec(92) = Wgt;
    WgtVec(100) = 100-Wgt;
    [PeakDiff,~,SR] = CV_Function(WgtVec);
    Peak_Diff_Vec(Wgt_Iter) = PeakDiff;
    Scan_Rate_Vec(Wgt_Iter) = SR;
    U_Wt_Vec(Wgt_Iter) = 100*WgtVec(92)/sum(WgtVec);
    Wgt_Iter = Wgt_Iter + 1;
    Wgt = Wgt + Wgt_Increment;
    if mod(Wgt_Iter,100) == 0
        disp(Wgt);
    end
end

Peak_Vs_Wt_Fig = figure;
plot(U_Wt_Vec,Peak_Diff_Vec);
xlabel('U Weight Percent (%)');
ylabel('Peak Difference (Amp)');
title('Peak Difference vs. U Weight Percent');
```

C.5 Data_Sweep.m

```
%This module takes the data within the Mass_ER variable and
   generates the
%CV peak current difference for each element in this variable.
   Mass_ER will
%need to be changed to out.Mass_ER if data is taken directly
   from an SSPM
%run.

Peak_Diff_Vec = zeros(size(Mass_ER,1),1);
Scan_Rate_Vec = zeros(size(Mass_ER,1),1);
U_Wt_Vec = zeros(size(Mass_ER,1),1);


for Time_Iter = 1:size(Mass_ER,1)
    WgtVec = Mass_ER(Time_Iter,:)';
    [Peak_Diff,Data_Select,SR] = CV_Function(WgtVec);
    Peak_Diff_Vec(Time_Iter) = Peak_Diff;
    Scan_Rate_Vec(Time_Iter) = SR;
    U_Wt_Vec(Time_Iter) = 100*WgtVec(92)/sum(WgtVec);
    if mod(Time_Iter,100) == 0
        disp(Time_Iter)
    end
end

Peak_Diff_Fig = figure;
plot(Peak_Diff_Vec);
hold on;
```

```
plot(Scan_Rate_Vec);
xlabel('Time (hr.)');
ylabel('Peak Difference (Amp)');
title('Peak Difference vs. Time');
Wt_Fig = figure;
plot(U_Wt_Vec);
xlabel('Time (hr.)');
ylabel('U Weight Percent (%)');
title('U Weight Percent vs. Time');
Peak_Vs_Wt_Fig = figure;
plot(U_Wt_Vec,Peak_Diff_Vec);
xlabel('U Weight Percent (%)');
ylabel('Peak Difference (Amp)');
title('Peak Difference vs. U Weight Percent');
```

C.6 CV_Plotting.m

```
%This module simply generates the plots which were used to show
    which
%extrapolation technique (constant or linear) was most
   appropriate for each
%input variable for the CV model.

Param_Names = ["Weight Percent"
         "ScanRate"
         "DoRev"
         "DRRev"
         "E0Cath1"
         "E0Anod1"
         "DoIrrev"
```

```
          "DRIrrev"
          "E0Cath2"
          "E0Anod2"
          "t\_init"
          "tRevCath"
          "tIrrevCath"
          "tIrrevAnod"
          "tRevAnod"
          "t\_interv"
          "Area"];
Param_Units = ["wt%"
          "mV/s"
          "cm^2/s"
          "cm^2/s"
          "V"
          "V"
          "cm^2/s"
          "cm^2/s"
          "V"
          "V"
          "s"
          "s"
          "s"
          "s"
          "s"
          "s"
          "cm^2"];
FitEqs = zeros(size(CV_Data,1)-1,2);
for i = 2:size(CV_Data,1)
    figure
```

```
    P1 = plot(CV_Data(1,:),CV_Data(i,:),'*');
    hold on;
    xlabel(sprintf("%s (%s)",Param_Names(1),Param_Units(1)));
    ylabel(sprintf("%s (%s)",Param_Names(i),Param_Units(i)));
    if i ~= 5  && i ~= 6 && i ~= 9 && i ~= 10 && i ~= 11 && i
       ~= 16
        A = polyfit(CV_Data(1,:),CV_Data(i,:),1);
        FitEqs(i,:) = A;
        P2 = plot(CV_Data(1,:),CV_Data(1,:)*A(1) + A(2));
        legend([P1,P2],["Data","Linear Fit"]);
    end
    title(sprintf("%s vs. U Weight Percent",Param_Names(i)))
    if i == 11
        Param_Names(i) = "t_init";
    elseif i == 16
        Param_Names(i) = "t_interv";
    end
    saveas(gcf,sprintf("%s Extrapolation.png",Param_Names(i)))
end
```

C.7 Extrapolation_Plots.m

```
%This module simply generates the plots which were used to show
    which
%extrapolation technique (constant or linear) was most
   appropriate for each
%input variable for the CV model.

Param_Names = ["Weight Percent"
         "ScanRate"
```

```
          "DoRev"
          "DRRev"
          "E0Cath1"
          "E0Anod1"
          "DoIrrev"
          "DRIrrev"
          "E0Cath2"
          "E0Anod2"
          "t\_init"
          "tRevCath"
          "tIrrevCath"
          "tIrrevAnod"
          "tRevAnod"
          "t\_interv"
          "Area"];
Param_Units = ["wt%"
          "mV/s"
          "cm^2/s"
          "cm^2/s"
          "V"
          "V"
          "cm^2/s"
          "cm^2/s"
          "V"
          "V"
          "s"
          "s"
          "s"
          "s"
          "s"
```

```
        "s"
        "cm^2"];
FitEqs = zeros(size(CV_Data,1)-1,2);
for i = 2:size(CV_Data,1)
    figure
    P1 = plot(CV_Data(1,:),CV_Data(i,:),'*');
    hold on;
    xlabel(sprintf("%s (%s)",Param_Names(1),Param_Units(1)));
    ylabel(sprintf("%s (%s)",Param_Names(i),Param_Units(i)));
    if i ~= 5  && i ~= 6 && i ~= 9 && i ~= 10 && i ~= 11 && i
       ~= 16
        A = polyfit(CV_Data(1,:),CV_Data(i,:),1);
        FitEqs(i,:) = A;
        P2 = plot(CV_Data(1,:),CV_Data(1,:)*A(1) + A(2));
        legend([P1,P2],["Data","Linear Fit"]);
    end
    title(sprintf("%s vs. U Weight Percent",Param_Names(i)))
    if i == 11
        Param_Names(i) = "t_init";
    elseif i == 16
        Param_Names(i) = "t_interv";
    end
    saveas(gcf,sprintf("%s Extrapolation.png",Param_Names(i)))
end
```

C.8 Stepwise_Fit.m

```
%This determined the linear fits in the CV data, for CV peak
   difference vs.
%uranium wt%.
```

```
Break_Points = [2.0,2.5,5.0,7.5,10.0];
CV_Fit_Mat = [];
CV_Invert_Fit_Mat = [];
Fit_Data = [];
j = 1;

for i = 1:length(Peak_Diff_Vec)
    if U_Wt_Vec(i) >= Break_Points(j) || i == length(
       Peak_Diff_Vec)
        Fit_Eqn = polyfit(Fit_Data(:,1),Fit_Data(:,2),1);
        CV_Fit_Mat = [CV_Fit_Mat;Fit_Eqn];
        Invert_Fit_Eqn = polyfit(Fit_Data(:,2),Fit_Data(:,1),1)
           ;
        CV_Invert_Fit_Mat = [CV_Invert_Fit_Mat;Invert_Fit_Eqn];
        Fit_Data = [];
        j = j + 1;
    else
        Fit_Data = [Fit_Data;[U_Wt_Vec(i),Peak_Diff_Vec(i)]];
    end
end
```

C.9 Gen_Fit_Uncertainty.m

```
%This module was designed to calculate the uncertainty in the
   linear fits
%found earlier by taking the output from the model and
   producing some
%normal random error around each data point. This was used to
   evaluate the
```

```
%influence of data uncertainty on the uncertainty of the
   regressions.

SweepTest;

Peak_Diff_Curr = Peak_Diff_Vec;
Break_Points = [2.0,2.5,5.0,7.5,10.0];
max_Err_Vec = [];

Peak_Rel_Uncertainty = 0.15;
Conv_Thresh = 0.001;
Conv_Check = 0;

Std_Dev_Slope = zeros(5,1);
Std_Dev_Slope_New = zeros(5,1);
Std_Dev_Intercept = zeros(5,1);
Std_Dev_Intercept_New = zeros(5,1);
CV_Fits = [];
Iter = 1;
max_Iter = 1000;

%This iterates and generates randomized datasets until the
   convergence
%criteria is met. Here, the convergence criteria is that the
   standard
%deviation of the slope and intercept values for each trend
   varies only a
%small amount when including an additional trend from another
   set of random
%data.
```

```
while Conv_Check > Conv_Thresh || Iter < 4
    if Iter > max_Iter
        break;
    end
    for i = 1:length(U_Wt_Vec)
        %Generates random numbers for each peak difference
        %rng('shuffle');
        Peak_Diff_Curr(i) = ( Peak_Rel_Uncertainty*
           Peak_Diff_Vec(i)*randn() )...
                              + Peak_Diff_Vec(i);
    end

    %Nearly identical to Stepwise_Fit.m It will generate the
       trends from
    %the random data.
    CV_Fit_Mat = [];
    CV_Invert_Fit_Mat = [];
    Fit_Data = [];
    j = 1;

    for k = 1:length(U_Wt_Vec)
        if U_Wt_Vec(k) >= Break_Points(j) || k == length(
           U_Wt_Vec)
            Fit_Eqn = polyfit(Fit_Data(:,1),Fit_Data(:,2),1);
            CV_Fit_Mat = [CV_Fit_Mat;Fit_Eqn];
            Invert_Fit_Eqn = polyfit(Fit_Data(:,2),Fit_Data
               (:,1),1);
            CV_Invert_Fit_Mat = [CV_Invert_Fit_Mat;
               Invert_Fit_Eqn];
            Fit_Data = [];
```

```
        j = j + 1;
    else
        Fit_Data = [Fit_Data;[U_Wt_Vec(k),Peak_Diff_Curr(k)
           ]];
    end
end

Reg = 1;
max_Err = 0;

%This will predict the uranium concentration from the peak
   difference
%givein in the random data, via reverse-correlating from
   the trends
%found earlier.
for m = 1:length(U_Wt_Vec)
    if U_Wt_Vec(m) > Break_Points(Reg)
        Reg = min(Reg + 1,5);
    end

    U_Wt_Predict = CV_Invert_Fit_Mat(Reg,1)*Peak_Diff_Curr(
       m)...
                  + CV_Invert_Fit_Mat(Reg,2);
    Perc_Diff = abs(U_Wt_Predict-U_Wt_Vec(m))/U_Wt_Vec(m);
    max_Err = max(max_Err,Perc_Diff);
end

max_Err_Vec = [max_Err_Vec,max_Err];

CV_Fits(:,:,Iter) = CV_Fit_Mat;
```

```
    CV_Invert_Fits(:,:,Iter) = CV_Invert_Fit_Mat;

    %This loop checks to see if the convergence criteria has
       been met.
    if Iter == 1
        Conv_Check = 0;
    elseif Iter == 2
        for n = 1:length(Break_Points)
            Std_Dev_Slope(n) = std(CV_Fits(n,1,:));
            Std_Dev_Intercept(n) = std(CV_Fits(n,2,:));
        end
        Conv_Check = 0;
    else
        for n = 1:length(Break_Points)
            Std_Dev_Slope_New(n) = std(CV_Fits(n,1,:));
            Std_Dev_Intercept_New(n) = std(CV_Fits(n,2,:));
        end
        Conv_Check_Slope = max(abs( (Std_Dev_Slope_New -
           Std_Dev_Slope)./Std_Dev_Slope_New) );
        Conv_Check_Intercept = max(abs( (Std_Dev_Intercept_New
           - Std_Dev_Intercept)./Std_Dev_Intercept_New) );
        Conv_Check = max(Conv_Check_Slope,Conv_Check_Intercept)
           ;
        Std_Dev_Slope = Std_Dev_Slope_New;
        Std_Dev_Intercept = Std_Dev_Intercept_New;
    end

    Iter = Iter + 1;

end
```

```
%Calculates the average of the maximum error found between the
   predicted
%and actual uranium weight percent.
Mean_Err = mean(max_Err_Vec);

mean_Slopes = zeros(5,1);
mean_Intercepts = zeros(5,1);

for i = 1:length(Break_Points)

    mean_Slopes(i) = mean(CV_Fits(i,1,:));
    mean_Intercepts(i) = mean(CV_Fits(i,2,:));

end

figure;

%These will later be used to make the heatmap
All_Slopes_Norm = [];
All_Intercepts_Norm = [];

%This plots the z-scores for the different slope and intercept
   values for
%each region to give a sense of the spread of the trends.
for n = 1:length(Break_Points)
    if n == 1
        MSpec = '*';
        CSpec = 'r';
    elseif n == 2
```

```
        MSpec = 'o';
        CSpec = [0.4660 0.6740 0.1880];
    elseif n == 3
        MSpec = 'd';
        CSpec = 'b';
    elseif n == 4
        MSpec = 'x';
        CSpec = 'm';
    else
        MSpec = '+';
        CSpec = 'k';
    end
    Slopes = squeeze(CV_Fits(n,1,:));
    Intercepts = squeeze(CV_Fits(n,2,:));
    All_Slopes_Norm = cat(1,All_Slopes_Norm,(Slopes-mean(Slopes
       ))/Std_Dev_Slope(n));
    All_Intercepts_Norm = cat(1,All_Intercepts_Norm,(Intercepts
       -mean(Intercepts))/Std_Dev_Intercept(n));

    plot( ( Intercepts - mean(Intercepts) )/Std_Dev_Intercept(n
       ) ,...
          ( Slopes - mean(Slopes) )/Std_Dev_Slope(n),'LineStyle
             ','none','Marker',MSpec,'Color',CSpec );
    hold on;
end

%set(gca,'color',[0.92,0.92,0.92]);

title('Slope vs. Intercept z-scores for Linear Trends');
xlabel('Intercept z-score');
```

```
ylabel('Slope z-score');
legend('<2 wt%', '2 to 2.5 wt%', '2.5 to 5 wt%', '5 to 7.5 wt
   %', '7.5 to 10 wt%');

%This makes the heat-map (or frequency plot) of the same z-
   score data, just
%in a different format.
figure;
hist3([All_Intercepts_Norm,All_Slopes_Norm],'CDataMode','auto
   ','Nbins',[50,50],'LineStyle','none');
title('Frequency Plot of Slope vs. Intercept z-scores');
xlabel('Intercept z-score');
ylabel('Slope z-score');
xlim([min(All_Intercepts_Norm),max(All_Intercepts_Norm)])
ylim([min(All_Slopes_Norm),max(All_Slopes_Norm)])
colorbar
grid off
view(2)
```

Vita

Jonathan Mitchell was born in 1995 in Knoxville, Tennessee to Ginger and Darrell Mitchell. He grew up in Knoxville, where he attended Farragut elementary, middle and high school. During high school, his teachers fostered his love for math and the sciences, which drove him towards obtaining a college degree. During his undergraduate years, he took classes in Nuclear engineering and Mathematics, and gained interest in the nuclear fuel cycle, radiation transport, and related topics. In graduate school, he continued his research work from his undergraduate years: developing models for measurement techniques that had promise for use in pyroprocessing safeguards for use in assessing their feasibility for future reprocessing installations. This led to a master's thesis on cyclic voltammetry, a technique used to measure the uranium content in the electrorefiner. Following his master's, he intends on continuing his education, followed by possible research work at a national lab and eventually teaching classes.